Doctoral Thesis

STUDY ON ORGANIC PIGMENTS

PREPARATION OF NOVEL AZO PIGMENTS AND CLARIFICATION OF THE EMITTING STATE OF A UNIQUE FLUORESCENT PIGMENT

September 2015

OTANI Junji

Doctoral Thesis reviewed
by Ritsumeikan University

STUDY ON ORGANIC PIGMENTS

PREPARATION OF NOVEL AZO PIGMENTS AND CLARIFICATION
OF THE EMITTING STATE OF A UNIQUE FLUORESCENT PIGMENT

有機顔料の研究

新規アゾ顔料の合成ならびに興味深い蛍光顔料の発光状態の解明

September 2015
2015 年 9 月

OTANI Junji
大 谷 淳 司

Principal Referee: Professor KIKUCHI Takeshi
主 査 ： 菊 地 武 司 教 授

To the Memory of My Late Father

Holistic Abstract

The author of the present thesis has been engaged in fundamental research and development of organic pigments at several companies as a researcher. Of a variety of the subjects he studied, it was felt that some of the results were worth integrating as a scientific thesis. This thesis consists of the following contents: Syntheses and properties of four novel azo pigments, and study on the emitting state of a scientifically interesting compound.

Azo pigments have been widely used in our life as the colorants which have low to moderate durability. Firstly, the author has attempted drastic modification of chemical structures of azo pigments to explore potential of azo pigments. The two pigments out of the above four have an additional substituent in contrast to the conventional azo pigments used for the comparable counterparts on the chemical structures. The pigments synthesized exhibited red hues resembling those of the counterparts, and durability (photo- and heat-stability) of them was improved. The optical absorption spectra of the pigments in solution showed a hyperchromic effect but no bathochromic shift. Involvement of the substituent in the optical properties was studied using molecular orbital (MO) calculation with geometry optimization for a hydrazone tautomer, where the azo moiety of azo pigments, in general, has tautomerism between azo (-N=N-) and hydrazone (-NH-N=) linkages. It was concluded that the substituent hardly joined in the π-conjugation systems and was involved in the electron transitions. The other two pigments were obtained from newly designed starting compounds aiming at black hue in the category of azo pigments through extension of the π-conjugation systems. The crystal structures of the pigments were successfully solved from powder X-ray diffraction data combined with DFT calculations. The pigment molecules comprise hydrazone configurations, and are highly planar in the crystal structures, suggesting that the molecules have the broad π-conjugation systems as expected. The transition dipoles of the pigments were arranged with oblique fashion, probably inducing Davydov Splitting, which is advantageous for black hue as well as the extended π-conjugation systems. The present syntheses for the novel azo pigments suggest creation of new subclasses in the category of azo pigment.

Organic fluorescent pigments are important materials for colorants together with azo ones. Solid state is, in general, inconvenient for fluorescent emission because the cohesive forces usually provide non-fluorescent deactivation processes, and thus

solid-state-fluorescent materials are scientifically of great interest. The author opted for a solid-state-fluorescent compound and studied its emitting state because the compound is unique in its excellent and practical photostability. Fluorescent behavior of the compound in some organic solvents of various polarities was studied using MO calculation, steady state and time-resolved spectroscopy. The fluorescence spectra of the compound were broad and structureless associating with an excimer emission, but the emission was ascribable to the deactivation from the LUMO of an isolated molecule to the HOMO, i.e. not an excimer emission. The LUMO has a non-zero dipole moment formed through intramolecular charge transfer (ICT) while excitation from the HOMO whose dipole moment is almost zero. The solvent polarities varied largely the fluorescence quantum efficiencies and moderately the radiative rate constants, although the absorption maxima were insensitive to the solvent polarities. Discussion on these results concluded that the emitting state of the compound is influenced by a solvent-dependent non-radiative deactivation process, for which solvent-sensitive intersystem-crossing can be proposed.

In conclusion, the author prepared four novel azo pigments through drastic modification of chemical structures of azo pigments, and investigated their fundamental properties. The results indicate that azo pigment, which is a historically old category, yet has had potential for further expansion of its horizons. Regarding the category of organic fluorescent pigments, the author investigated a scientifically interesting organic solid-state-fluorescent compound in detail, and clarified its emitting state. The outcome of the present thesis will be useful information for research and development of functional colorants.

CONTNETS

Chapter 3: Synthesis and Structure Determination from Powder X-ray Diffraction Data of Black Azo (Hydrazone) Pigments

Chapter 1

General Introduction [1,2]

In this chapter, general information concerning pigments is concisely provided as preparation for the succeeding chapters. The following subjects are included: Definition of colorant, applications of pigments, classification of pigments, azo pigments, fluorescent pigments, and topics concerning hue. Finally, scope of the present thesis is summarized.

1.1 Colorant: Pigments and dyes

Colorant is a material that imparts color to materials. In general, colorant is largely classified into pigments and dyes. These classes of colorant are distinguished typically by solubility to solvents. Dyes are easily dissolved in solvents, water, for example. Dyes are therefore used in a molecularly dispersed condition in media, and the nature of dye molecules almost determines hue in the media. In contrast, pigments have low solubility to solvents or are almost insoluble. Pigments are used in a dispersed condition in media in which fine solid particles (agglomerates[1]) of the pigment molecules (aggregates[2]) are dispersed [1]. Optical properties originated from a single pigment molecule are modified by crystal polymorphism, if any, in the aggregate. Hue of the pigment is also altered through conditions of the agglomeration and dispersion in the media, and is therefore determined by the conditions of aggregation, agglomeration and dispersion of the pigment particles with their shape, size and distribution, rather than the nature of the isolated single molecule. A crystalline state, in general, is a condition energetically more stabilized and inert than a molecular state, and pigments are usually more durable than dyes, e.g., resistivity to light and heat better than those of dyes. Table 1 quickly compares pigments and dyes according to some characteristics including the properties described the above.

[1] Agglomerate: A form of a (pigment) particle comprising jumbled single crystals or primary particles (aggregate) which consist of the single crystals of the pigment, separable by dispersion processes.

[2] Aggregate: A primary particle consisting of (pigment) single crystals, unable to be broken down by dispersion processes.

Table 1 General comparison between pigments and dyes

Characteristics	Pigments	Dyes
• Origin of color in use	• Agglomerated colored molecule dispersed in a medium	• Colored molecule molecularly dispersed in a medium
• Factors modifying color	• Crystal polymorphism • Shape, size and distribution of agglomerated pigment particles • Dispersion states of agglomerated pigment particles	• Interaction with a solvent and/or a medium
• Solubility to solvents	• Low or insoluble	• Easily soluble
• Durability of color	• Excellent	• Poor
• Dispersion into media	• Elaborative	• Easy

1.2 Applications of pigments

Reportedly, use of pigments by the human race dates from cave or body paintings drawn in pre-Christian Egypt, China, France or somewhere. Ever since, people have utilized pigments for the very simple purpose of giving color to personal or public belongings in order simply to enjoy life making it richer, safer, more joyful, distinguishable and less drab. In industry, applications of pigments are mostly three-fold, i.e., coloration for printing inks, coating paints, and plastics including synthetic fibers. In addition to the above principal applications, nowadays, pigments are utilized also for so-called “high-tech” applications such as photoconductors for electrophotography, color filters for liquid crystal displays, electro-luminescent diodes, ink-jet printing inks, and pigment-sensitized solar cells [3]. Pigments have been one of requisite materials in our life used for from conventional coloration to specific state-of-the-art applications.

1.3 Classification of pigments

Pigments are largely divided into inorganic and organic ones. Representative inorganic pigments derive originally from minerals, and include carbon black, titanium dioxide, iron oxides, zinc oxide, natural or synthesized oxides or salts of cadmium, cobalt, strontium, chromium, bismuth, molybdenum, vanadium etc. Organic pigments are the organic compounds which exhibit color, i.e., substances comprising atoms of carbon, oxygen, nitrogen etc. to partially or entirely constitute a chromophore. Relatively large π-conjugation system comprising these atoms can be a chromophore if the system has an optical absorption band in a visible wavelength region. Some of organic pigments contain metal ions for the purpose of insolubilization (formation of salts or metal complexes). Organic pigments are the majority in production and

application compared with inorganic pigments because use of the heavy metals contained in inorganic pigments, such as cadmium and chromium, tend to be avoided mainly due to environmental reasons [1].

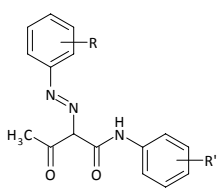

Monoazo Yellow and Orange

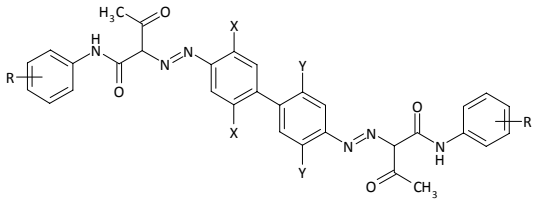

Disazo (diarylide) Yellow

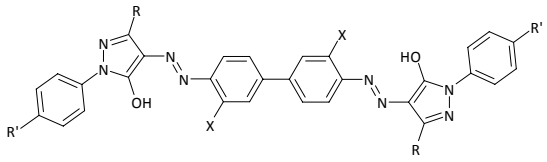

Disazopyrazolone

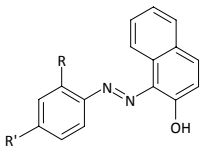

β-Naphthol

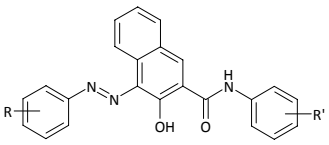

Azonaphtharylamide (Naphthol AS)

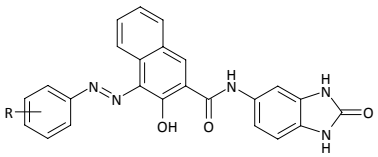

Benzimidazolone

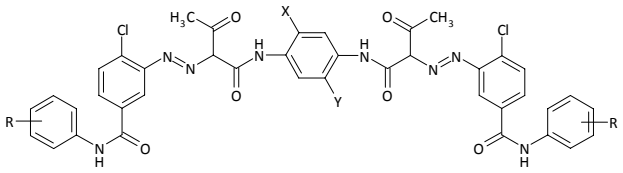

Disazo Condensation

Figure 1 Chemical structures of some typical azo pigments. Subclasses depicted under each chemical structure are the common names conventionally established in colorant industry. In the structures, R, R', X and Y represent the substituents and are solely indicated without details such as concrete chemical groups and positions. Azo pigments containing metals are excluded, e.g., lake (salt) and metal complex pigments.

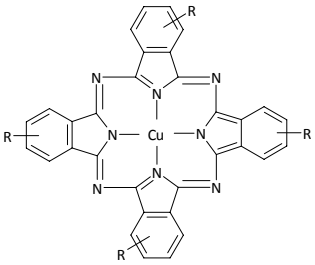

Copper Phthalocyanine

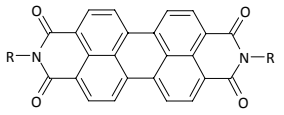

Perylene

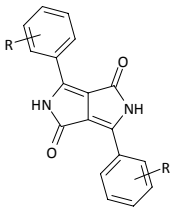

Diketopyrrolopyrrole

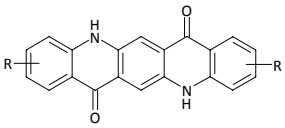

Quinacridone

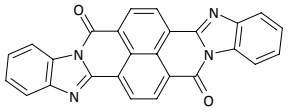

Perinone

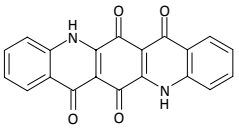

Quinacridone Quinone

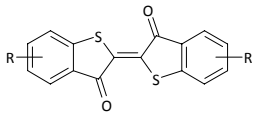

Thioindigo

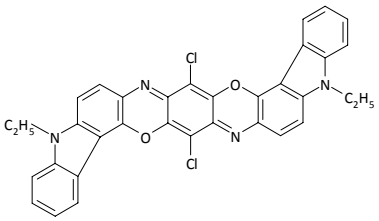

Dioxazine

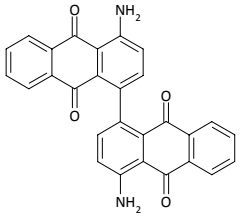

Aminoanthraquinone

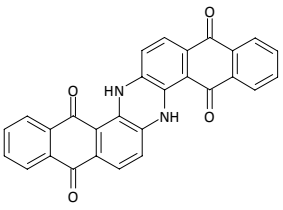

Indanthrone

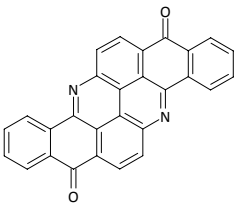

Flavanthrone

Figure 2 Chemical structures of some typical polycyclic pigments. Subclasses depicted under each chemical structure are the common names conventionally used in colorant industry. In the structures, R represents the substituent and is solely indicated without details such as concrete chemical groups and positions.

1.4 Organic pigments

Organic pigments include natural and synthetic ones, and the latter dominates industry of production and application. Organic pigments are further subdivided into azo pigments having azo linkage (-N=N-)[3] and polycyclic pigments. Both azo and polycyclic pigments constitute a variety of subclasses, and chemical structures of some of them are summarized in Figures 1 and 2 as the representative examples.

Azo pigments were developed in the second half of the nineteenth century. The pigments can be economically produced as described in the next section, and exhibit typically yellow, orange and red to brown colors. Some of azo pigments are known to exhibit photoconductivity, and have been commercially applied for organic photoconductors (OPC) of electrophotographic copying machines [3]. Polycyclic pigments consist of heteroaromatic systems, and include metal or metal-free phthalocyanines, perylenes, diketopyrrolopyrroles, quinacridones, perinone, thioindigos, aminoanthraquinone, dioxazine etc. (Figure 2). These are the common names conventionally used in colorant industry. Some of polycyclic pigments cover green and blue which are the hues commercially difficult to obtain by azo pigments. Apart from phthalocyanine pigments, most of polycyclic pigments are more costly than azo pigments in production [1]. It has been known that specific crystal phases of copper phthalocyanine or specific derivatives of perylene and diketopyrrolopyrrole show photoconductivity and other electronic properties. These are applicable for OPC and other electronic applications such as light-emitting diode and gas sensors [3-6].

In general, polycyclic pigments are more excellent than azo pigments in durability. Consequently, application fields where require extraordinary weatherability, e.g., coating paints for automobiles, tend to use polycyclic pigments, some of which, in this respect, are often grouped as “high-performance pigments” [7]; and the fields where require moderate durability, e.g., printing inks and plastics for stationery, tend to choose azo pigments, some of which, in contrast, often called as “mid- to low-performance pigments”.

1.5 Azo pigments

Azo pigments were developed after discovery of formation of a diazonium salt obtained from a primary amine in 1858 [2]. The pigments can be economically

[3] Azo linkage can have the other linkage, hydrazone (-NH-N=), by a tautomerism, and the term “azo” has been conventionally used in colorant industry. Crystal structure analyses have revealed that many of the azo pigments analyzed to date exhibit “hydrazone” tautomer rather than “azo” tautomer.

produced through the standardized sequence of a diazonium salt formation from an aromatic amine and a subsequent reaction with a wide choice of a coupling component (Scheme 1). Various kinds of the coupling components mainly led development of a variety of azo pigments. In accordance with market demands for coloration, e.g., color variations and practical performances, lots of azo pigments were developed during the late 19th to middle 20th centuries. Accordingly, a variety of subclasses of azo pigments were formed; such as monoazo yellow, monoazo orange, disazo yellow, disazopyrazolone, β-naphthol, azonaphtharylamide, benzimidazolone, disazo condensation and so on (Figure 1). These are the common names conventionally established in colorant industry. The category of azo pigments includes those containing metals, i.e., lakes and metal complexes. Azo lakes are the metal salts made with carboxylic and/or sulfonic acid part(s) in the structures, and azo metal complex pigments are those whose metals coordinate to the nitrogen atoms in the azo linkages as the ligands.

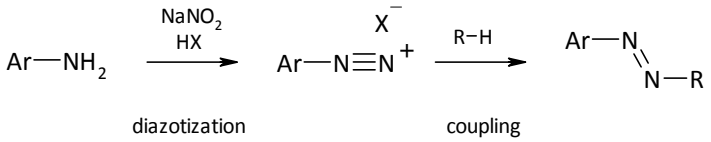

Scheme 1 General synthetic procedure of azo pigment.

Of more than 150 red organic pigments which are commercially available and whose Color Index Generic Names and Constitution Numbers[4] are given [1], azonaphtharylamide type pigments account for nearly one third of the 150, suggesting that this subclass has been one of the most important red pigments in colorant industry. Those pigments are obtained by coupling substituted aryl diazonium salts with arylides of 2-hydroxy-3-naphthoic acid for the coupling components (“Naphtol AS” as the industrial common name). They provide a broad range of red colors from yellowish and medium to bluish red covering brown and violet shades. Although their solvent fastness and migration resistance are only marginal, azonaphtharylamide type pigments have been used mainly in printing inks and paints mostly as mid- to low-performance pigments [1].

[4] Color Index International (C.I. in abbreviation) is the reference database of colorant jointly made and maintained by the Society of Dyes and Colourists and the American Association of Textile Chemists and Colorists. The database includes the list of more than 6000 colorants (both dyes and pigments) with Color Index Generic Names based on the hues and Color Index Constitution Numbers based on the chemical structures.

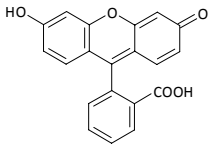

Fluoreceine

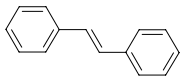

Stilbene

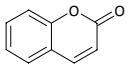

Coumarin

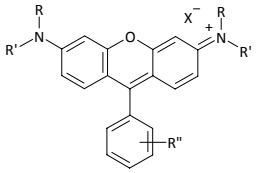

Rhodamine

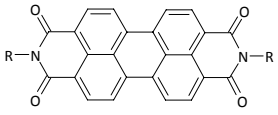

Perylene

Figure 3 Examples of typical fluorophores. The names of the compounds depicted under each chemical structure are the common names conventionally used. In the structures, R, R' and R" represent the substituent and are solely indicated without details such as concrete chemical groups and positions.

1.6 Fluorescent pigments

The category "fluorescent pigments" is often made for the classification of pigments besides the classes of inorganic and organic ones. Absorption, scattering and reflection of light are the principles that general inorganic and organic pigments exhibit colors, whereas emission of light is the fundamental and distinct principle for fluorescent pigments to exhibit colors. Fluorescent pigments include inorganic and organic ones.

Inorganic fluorescent pigments comprise host crystals of metal oxides or sulfides doped with other metals, e.g., $SrAl_2O_4$:Eu, Y_2O_3:Eu, ZnS:Ag, and ZnS:Cu etc. These are used by dispersion typically in a transparent and colorless medium, plastic, for example. Organic fluorescent materials include derivatives of aromatic fluorophores such as fluorecein, stilbene, coumarin, rhodamines and perylenes (Figure 3). These organic compounds are essentially soluble, i.e., not pigment in terms of solubility, and are dissolved in a transparent medium because these molecules efficiently fluoresce in a molecularly dispersed state. The solid solutions thus prepared are then ground into fine particles for dispersion of paints, printing inks or plastics, like agglomerated pigment particles. Inorganic and organic fluorescent pigments in the media give off colors with a

remarkable vivid brilliance due to their spontaneous emission upon excitation by light exposure or irradiation. The pigments are, therefore, applied for visibility purposes to attract attention such as decorative advertisements, dials for clocks, and the fields of safety, e.g., road markings, signs for traffic and emergency evacuation etc.

It should be noted here that, among various organic fluorescent compounds, there exist some molecules which can fluoresce even in the solid state, while intermolecular interactions work usually as cohesive forces for the molecules to be solid, and the interactions make the compounds be less- or non-fluorescent providing non-radiative deactivation paths. Such molecules are of great interest in terms of their emitting states. Solid-state-fluorescent compounds include metal complexes of hydroxyquinoline, derivatives of diketopyrrolopyrrole, hydroquinone, oxazoles, phenazine etc., and are applicable for organic light-emitting diodes or optical memories [8-10].

1.7 Color mixing

The most fundamental purpose of pigments is coloration, and the most essential functionality of pigments is therefore hue. A vast variety of hues (colors) can be created by mixing colors. There are two laws of color mixing, i.e., additive color mixing and subtracting color mixing [2].

Additive color mixing concerns light, and the three primary colors of light, i.e., red, green and blue (RGB) can synthesize any colors through transparently mixing two or more of the three colors as shown in the left of Figure 4. Lightness of the hue increases upon mixing since the amount of light is incremented through transmittance of the light. The equivalent mixture of the three colors produces white. Additive color mixing is used for producing full-color typically in liquid crystal displays through RGB color filters.

Subtractive color mixing concerns colorant, and the three primary colors of colorant, i.e., yellow, magenta and cyan (YMC) can provide also any colors through reflectionally mixing two or more of the three colors as shown in the right of Figure 4. Lightness of the hue decreases upon mixing since the amount of the light is decremented through absorption of the light. The equivalent mixture of the three colors produces black in contrast to additive color mixing. Subtractive color mixing is routinely used in colorful printings through full-color ink-jet printers, for example.

In principle, any kinds of colors can be obtained by using additive mixing or subtractive mixing. Nevertheless, most of commercially available ink-jet printers are equipped with an additional plurality of color inks besides YMC inks such as black,

light magenta and light cyan. Regarding liquid crystal displays, cyan and yellow color filters have been proposed in addition to the RGB filters to improve reproducibility of yellow, gold and pale blue [11]. The above additional colors are provided in pursuit of precise color reproducibility from original color images. Furthermore, processes of mixing the primary colors are not always easy to exactly reproduce intended hue with saturation. The three primary colors are hence never enough for coloration, and colorants exhibiting colors other than the three primary colors are therefore indispensable for various applications, e.g., colorant for black, white, orange, brown, purple etc.

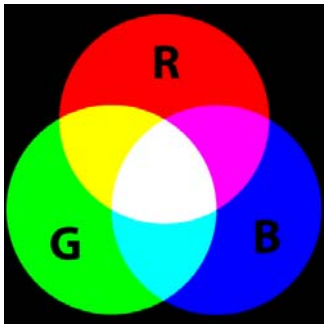

Additive color mixing

R: Red, G: Green, and B: Blue

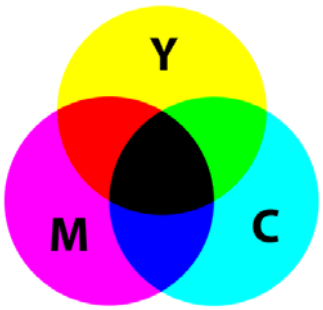

Subtractive color mixing

Y: Yellow, M: Magenta, and C: Cyan

Figure 4 Color mixing by three primary colors.[5]

1.8 White and black pigments

In general, pigments absorb light of specific wavelengths in visible light region, and we perceive the light which is not absorbed by the pigment as the color of the pigment. Ideally white pigment does not absorb any light of visible wavelength region. On the contrary, black pigment absorbs most of light in visible wavelength region. These colors are routinely used such as coating paints of automobile bodies, letter printings for books and newspapers. While white and black can be theoretically produced by additive and subtractive mixings, respectively, obtaining white and black by the mixings is however non-economical and unproductive. The two colors are neutral and monotonous but irreplaceable and distinct from other hues, and the pigments exhibiting white or black are the requisites.

[5] The figures were copied from the free encyclopaedia WIKIPEDIA. See “Additive color” and “Subtractive color”, respectively.

Inorganic white pigments include titanium dioxide, zinc oxide, magnesium oxide, and barium sulfate. Of these, rutile-type titanium dioxide is most important as the principal white pigment. Derivatives of alkylenebismelamine are proposed as organic white pigments [12]. Hollow particles comprising polymers of various polymerization degrees for the shell are other examples of organic white pigments [13].

Black pigments include carbon black, graphite, iron (II) iron (III) oxide (magnetite), and composite oxides comprising copper and chromium, or copper, chromium and zinc. Some perylene derivatives are known for exhibiting black [14]. Of the above pigments, carbon black is predominant in terms of production cost and extraordinary stability, although carbon black contains by-products, benzpyrene, for example, which has been known for a carcinogen.

1.9 Scope of the thesis

1.9.1 Purpose of the present study on organic pigments

Organic pigments are useful and indispensable materials for our life. In particular, azo pigments have been widely used in their long history as synthetic organic pigments. Drastic modification in chemical structures of azo pigments would be useful for exploring potential of azo pigments. One of the purposes of the present study on organic pigments is to substantiate that drastic chemical modifications can provide novel azo pigments with some functionality.

Organic fluorescent pigments are one of the industrially important categories of pigments. The pigments which fluoresce in the solid state are particularly interesting from a scientific point of view. Another purpose of the present study is to investigate the emitting state of a solid-state-fluorescent pigment. The compound the author opted for is a polycyclic fluorescent pigment and is unique in terms of its practical photostability, while most of fluorescent compounds are usually not stable due to their relatively long life in the excited state.

1.9.2 Synthesis of novel red azonaphtharylamide pigments

Azonaphtharylamide pigments constitute a commercially important subclass in azo pigments. The pigments are obtained using coupling components derived from 3-hydroxy-2-naphthoic acid. Alteration of the above mono-carboxylic acid to a dicarboxylic acid has not been attempted and will lead exploration for a new subclass of

azo pigments. Chapter 2 of the present thesis describes synthesis of two novel red azonaphtharylamide-type pigments using a coupling component starting from 3-hydroxy-2,7-naphthalene dicarboxylic acid. Presence of 7-substituent distinguishes the pigments from conventional azonaphtharylamide pigments. The following properties of the 7-substituted pigments are studied comparing with those of the conventional 7-unsubstituted counterparts; optical absorption and influence of the 7-substituent upon optical absorption using molecular orbital (MO) calculation with geometry optimization for a hydrazone configuration.

1.9.3 Synthesis of novel black azo pigments

One of the most important black pigment in industry is carbon black. This pigment boasts of its extraordinary durability and economical production, while this is carcinogenic due to impurities contained through its production process. Electric conductivity is another issue of the pigment in the application for liquid crystal displays. These drawbacks mainly lead a demand for a new black pigment. In general, extension of a π-conjugation system provides narrowing of the HOMO-LUMO gap and increments the number of bonding and anti-boding π-electron molecular orbitals, thereby inducing red shift of optical absorption and hopefully band broadening in the visible light region. Chapter 3 of the present thesis describes that novel black pigments can be produced in the category of azo pigment through extension of a π-conjugation system. 3-Hydroxy-2-naphthoic acid and 3-hydroxy-2,7-naphthalene dicarboxylic acid are used for the starting materials. The crystal structures of the pigments obtained are solved by ab initio powder X-ray diffraction analysis with DFT calculation. The results show that the black is materialized by the flat and broad π-conjugation systems probably assisted by a specific intermolecular interaction Davydov splitting.

1.9.4 Optical properties of a unique polycyclic fluorescent pigment

Of some organic fluorescent pigments which can fluoresce in the solid state, 1,2,3,4-tetrachloro-11H-isoindolo-[2,1-a]-benzimidazol-11-one (TCIB) is known for a unique and distinct compound in terms of its excellent and practical photostability [15]. Chapter 4 of the thesis discusses fluorescent behavior of TCIB in some organic solvents of various polarities using MO calculation, steady state and time-resolved spectroscopy to clarify the emitting state.

Chapter 2

Synthesis and Properties of Azonaphtharylamide Pigments Having Arylamide Groups at 2- and 7-Positions

2.1 Abstract

Two azonaphtharylamide pigments having arylamide groups at the 2- and 7-positions on the naphthol ring were synthesized and studied. Presence of the 7-substited amide group distinguishes the pigments from conventional azonaphtharylamide pigments derived from 3-hydroxy-2-naphthoic acid. The 7-substituent caused a hyperchromic effect but did not produce bathochromic shift in the optical absorption spectra in solution compared with the corresponding 7-unsubstituted counterparts. Molecular geometry optimizations through semi-empirical MO calculations showed that extent of the chromophore systems in the pigments with and without the 7-substituent is nearly the same, which is consistent with absence of the bathochromic shift. The MO calculations also showed that the MOs localized in 7-substituents are involved in the electronic transitions in the longest wavelength bands of the pigments, which is responsible for the hyperchromic effect. The 7-substituted pigments exhibited better resistivity to light and heat than the 7-unsubstituted ones.

2.2 Introduction

An important class of industrial azo pigments is synthesized using hydroxynaphthalene (β-naphthol) and its derivatives as a base for coupling components [1,2]. Of the derivatives, 3-hydroxy-2-naphthoic acid is one of the most important starting materials. The naphthalene ring of the naphthoic acid is a conjugated polyene and forms the central structure of the chromophore in the resultant pigments. The carboxylic acid at the 2-position has been utilized for the syntheses of a variety of coupling components through a simple amidation procedure. As a consequence of this, the industrially important subclasses of azo pigments, e.g., azonaphtharylamide-type and benzimidazolone-type, have been developed [1]. If an additional carboxylic acid is introduced to the naphthalene ring, further development of new azo pigments becomes possible. Synthesis of coupling components having amide groups at the 2- and 7-positions of the naphthol was, therefore, attempted to develop new azonaphtharylamide-type pigments. For this purpose, 3-hydroxy-2,7-naphthalene dicarboxylic acid **1**, as shown in Figure 1, was employed as the starting compound. This compound enables introduction of the same or mutually different substituents at the 2- and 7-positions through double amidation, which will allow development of a new subclass of azo pigments. It is expected that the substituent at the 7 position may impart functionality to the pigments and improve their technical performance. The author engaged in development of some of the

pigments synthesized from **1** [16,17]. Here, synthesis and fundamental properties of two kinds of the azo pigments are reported. As the coupling component, 3-hydroxy-N2,N7 -diphenyl-naphthalene-2,7-dicarboxamide **2** (Figure 1) was used because of its structural simplicity. Concerning the properties of the pigments, the effect of the 7-substituents upon the optical properties and chemical stabilities were investigated.

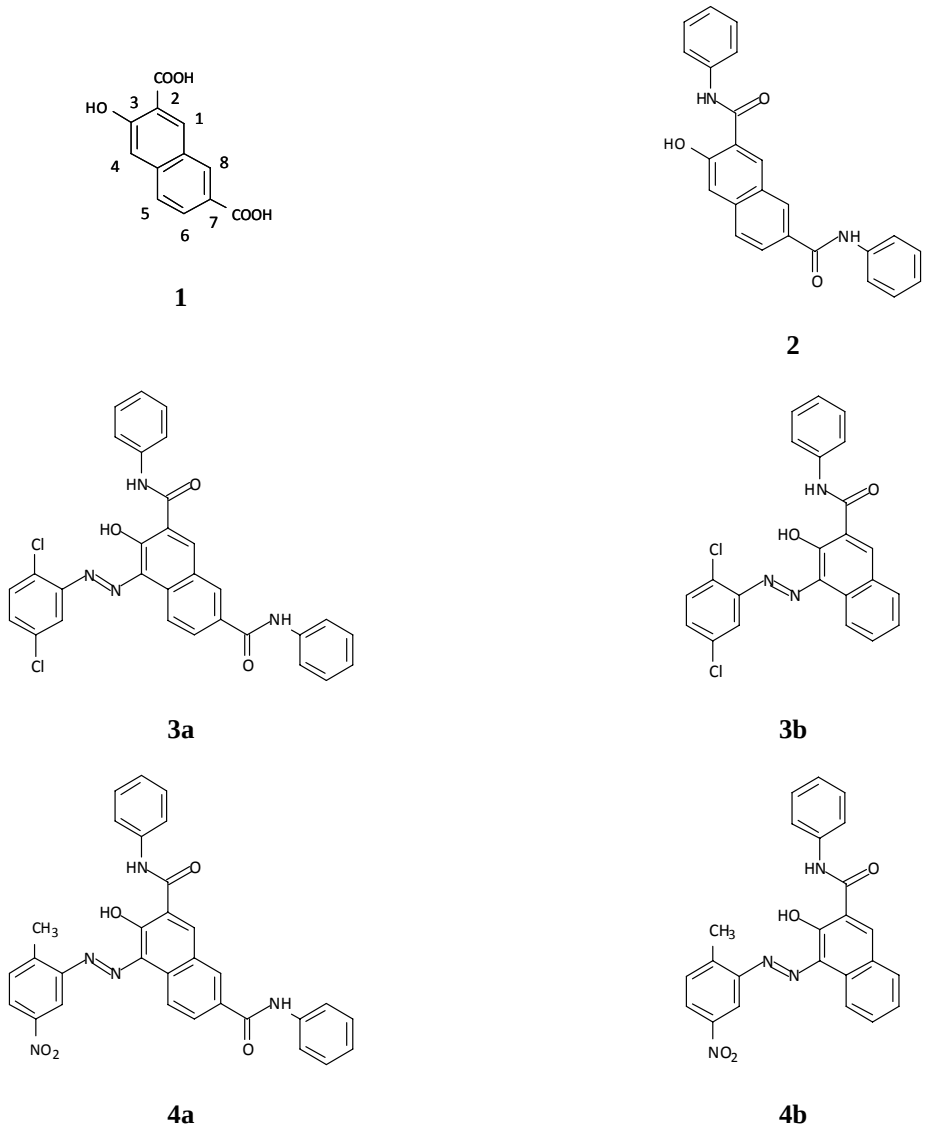

1 **2** **3a** **3b** **4a** **4b**

Figure 1 Chemical structures of starting compound **1**, coupling component **2** derived from **1**, azo pigments **3a** and **4a**, which were synthesized from **2**; and **3b** (C. I. Pigment Red 2) and **4b** (C. I. Pigment Red 22) used as reference. For easy comparison with **2**, the structures of **3a**, **3b**, **4a** and **4b** are depicted in the hydroxy-azo configurations, although they are believed to have the keto-hydrazone configurations.

2.3 Target materials

Figure 1 summarizes all the chemical structures of the materials used in the present study. The starting material is 3-hydroxy-2,7-naphthalene dicarboxylic acid **1**. 3-Hydroxy-N2,N7 -diphenylnaphthalene-2,7-dicarboxamide **2** is the coupling component (intermediate) synthesized form **1**. The new 7-substituted azonaphtharylamide pigments having two arylamide substituents derived from **2** are 4-(2,5-dichlorophenyl)azo-3-hydroxy-N2,N7 -diphenylnaphthalene-2,7-dicarboxamide (**3a**) and 4-(2-methly-5-nitrophenyl)azo-3-hydroxy -N2,N7-diphenylnaphthalene-2,7-dicarboxamide (**4a**). Figure 1 shows also the counterparts of **3a** and **4a**, i.e., 4-(2,5-dichlorophenyl)azo -3-hydroxy-N-phenylnaphthalene-2-carboxamide (C.I. Pigment Red 2, **3b**) and 4-(2-methyl-5-nitrophenyl)azo-3-hydroxy-N-phenylnaphthalene -2-carboxamide (C.I. Pigment Red 22, **4b**); the 7-unsubstituted conventional azonaphtharyl -amide pigments having one arylamide substituent for comparison. As discussed later, a tautomerism can exist between the structures of azo (–N=N-) and hydrazone (–NH-N=) in **3a**, **3b**, **4a** and **4b**, and the structures of these pigment molecules are depicted in the azo configurations for easy comparison with **2**, although they are believed to have the hydrazone configurations.

2.4 Experimental

2.4.1 Materials

All the chemicals were purchased from Tokyo Kasei Co., Ltd. except 3-hydroxy-2,7 -naphthalene dicarboxylic acid. The dicarboxylic acid was purchased from Wako Pure Chemical Industries. Solvent-soluble acrylic resin BR-87 was obtained from Mitsubishi Rayon Co., Ltd.

2.4.2 Instruments

Decomposition points were measured with Bruker TG-DTA2000SA. Mass spectra were taken on JEOL JMS-700 (EI-TOF MS) and Bruker Ultraflex TOF/TOF MS (MALDI-TOF MS). ^{1}H and ^{13}C NMR spectra were recorded on a JEOL JNM-ECS400 Spectrometer. UV-Vis absorption spectra were measured with HITACHI U-3310 Spectrophotometer. Powder X-ray diffraction patterns were evaluated with Rigaku MiniFlex600 (Cu K_{α}, 30kV/15mA). Light fastness of the pigments was evaluated with ASAHI Spectra Solar Simulator HAL-320.

*2.4.3 Synthesis of 3-hydroxy-N2,N7-diphenyl-naphthalene-2,7-dicarboxamide (**2**)*

Slurry was made using 3-hydroxy-2,7-naphthalene dicarboxylic acid (20.0 g, 0.09 mol)

with 80 g of toluene. Aniline (48.1 g, 0.52 mol) was dissolved in 125.0 g of toluene at room temperature. Phosphorus trichloride (11.8 g, 0.09 mol) was added dropwise to the aniline solution and the mixture was filtrated. The filtrate obtained was then poured into the slurry and the reaction mixture was kept at 110°C for 3 hours while stirring, and then filtrated. The white powder, 3-hydroxy-N2,N7-diphenyl-naphthalene-2,7-dicarboxamide, was washed with methanol. Yield was 29.0 g (84.2 mol% relative to 3-hydroxy-2,7-dicarboxylic acid); ^{1}H NMR (400 MHz, DMSO-d6) δ 7.12 (t, 2H, *J* = 7.4 Hz), 7.16 (t, 2H, *J* = 7.4 Hz), 7.38 (t, 2H, *J* = 7.4 Hz), 7.40 (t, 2H, *J* = 7.4 Hz), 7.42 (s, 1H), 7.79 (d, 2H, *J* = 7.4 Hz), 7.83 (d, 2H, *J* = 7.4Hz), 7.90 (d, 1H, *J* = 7.6 Hz), 8.04 (dd, 1H, *J* = 7.6 Hz, 1.8 Hz), 8.61 (d, 1H, *J* = 1.8 Hz), 8.61 (s, 1H). ^{13}C NMR (100 MHz, DMSO-d6) δ 110.36, 120.22, 120.25, 123.38, 123.52, 123.97, 125.72, 125.86, 126.34, 128.54, 128.73, 128.96, 129.90, 131.58, 136.93, 138.39, 139.16, 155.05, 165.02, 165.24.

*2.4.4 Preparation of 2,5-dichloroaniline diazonium fluoroboric salt for 4-(2,5-dichlorophenyl)azo-3-hydroxy-N2,N7-diphenylnaphthalene-2,7-dicarboxamide (**3a**) and 4-(2,5-dichlorophenyl)azo-3-hydroxy-N-phenylnaphthalene-2-carboxamide (**3b**)*

2,5-Dichloroaniline (12.5 g, 0.08 mol) was put into a flask (300 ml) with 62.5 g of water and acetic acid (4.6 g, 0.08 mol). 35% Hydrochloride (16.1 g, 0.15 mol) was added dropwise to the above mixture keeping at 50°C. 35% Hydrochloride (16.1 g, 0.15 mol) and 50.0 g of water was then further added at 45°C. After cooling the system below 0°C, 16% of aqueous solution of sodium nitrite (0.08 mol) was added dropwise to the system while stirring. After removal of insoluble substances and wash with 12.5 g of water, the intermediate was kept below 5°C, and 42% fluoroboric acid (30.4 g, 0.16 mol) was added dropwise, and then filtrated. The precipitate was washed with water and subsequently with isopropyl alcohol, and dried. White crystalline powder was obtained. The yield was 17.8 g (98.7%). The salt was used for following diazotization without identification.

*2.4.5 Preparation of 2-metyl-5-nitoroaniline diazonium fluoroboric salt for 4-(2-methly-5-nitrophenyl)azo-3-hydroxy-N2,N7-diphenylnaphthalene-2,7-dicarboxamide (**4a**) and 4-(2-methyl-5-nitrophenyl)azo-3-hydroxy-N-phenylnaphthalene-2-carboxamide (**4b**)*

2-Methyl-5-nitroaniline (12.5 g, 0.08 mol) was put into a flask (300 ml) with 125.0 g of water and 25.7 g of 35% hydrochloride. 16% Sodium nitrite (39.0 g, 0.09 mol) was added dropwise to the above mixture keeping the system below 5°C. After removing insoluble substances, the intermediate was kept below 5°C, and 42% fluoroboric acid (32.4 g, 0.17 mol) was added dropwise, and then filtrated. The precipitate was washed with water, and subsequently isopropyl alcohol, and dried. White crystalline powder was obtained. The yield was 19.8 g (98.4%). The salt was used for following diazotization without identification.

*2.4.6 Synthesis of 4-(2,5-dichlorophenyl)azo-3-hydroxy-N2,N7-diphenylnaphthalene-2,7-dicarboxamide (**3a**)*

3-Hydroxy-N2,N7-diphenyl-naphthalene-2,7-dicarboxamide (3.0 g, 0.008 mol) was charged into a flask (100 ml) with N-methylpyrrolidone (NMP, 24.0 g) and sodium hydroxide (0.69 g, 0.017 mol). The mixture was stirred at 40°C and then cooled below 5°C. After 2,5-dichloroaniline diazonium fluoroboric salt (2.46 g, 0.009 mol) had been added to the flask while stirring and keeping the temperature below 5°C, the solution was stirred overnight at room temperature, and neutralization using acetic acid was performed. The red powder generated was filtrated and washed sequentially with acetone, methanol and water. Finally, the powder was dispersed in methanol, filtrated, and dried in an oven at 80°C. The powder thus obtained (2.6 g, 0.005 mol) was further treated in N,N-dimethylformamide (DMF, 20 g) at 120-130°C for 3 hours while stirring. The product was washed with DMF and methanol and dried in an oven at 80°C. Yellowish red 4-(2,5-dichlorophenyl)azo-3-hydroxy-N2,N7 -diphenylnaphthalene-2,7-dicarboxamide (2.2 g) was obtained as an extremely insoluble crystalline powder. Yield 50.5%; decomposition point 339°C; MALDI-TOF MS *m/z* 553.040 $[M-H]^-$ (100%), calcd for $[C_{30}H_{19}Cl_2N_4O_3]^-$ 553.083.

*2.4.7 Synthesis of 4-(2-methly-5-nitrophenyl)azo-3-hydroxy-N2,N7-diphenylnaphthalene-2,7-dicarboxamide (**4a**)*

3-Hydroxy-N2,N7-diphenyl-naphthalene-2,7-dicarboxamide (3.0 g, 0.008 mol) was charged into a flask (100 ml) with NMP (24.0 g) and sodium hydroxide (0.69 g, 0.017 mol). The mixture was stirred at 40°C and then cooled below 5°C. After 2-methyl-5-nitroaniline diazonium fluoroboric salt (2.36 g, 0.009 mol) had been added to the flask while stirring and keeping the temperature below 5°C, the solution was stirred overnight at room temperature, and neutralization using acetic acid was performed. The red powder generated was filtrated and washed sequentially with acetone, methanol and water. Finally, the powder was dispersed in methanol, filtrated, and dried in an oven at 80°C. The powder thus obtained (2.6 g, 0.005 mol) was further treated in DMF (20 g) at 120-130°C for 3 hours while stirring. The product was washed with DMF and methanol and dried in an oven at 80°C. Bluish red 4-(2-methly-5 -nitrophenyl)azo-3-hydroxy-N2,N7-diphenylnaphthalene-2,7-dicarboxamide (2.4g) was obtained as an extremely insoluble crystalline powder. Yield 56.1%; decomposition point 320°C; MALDI-TOF MS *m/z* 544.120 $[M-H]^-$ (100%), calcd for $[C_{31}H_{22}N_5O_5]^-$ 544.162.

The following syntheses of **3b** and **4b** were carried out to obtain chemically pure samples. Commercially available ones may contain additives such as dispersants.

*2.4.8 Synthesis of 4-(2,5-dichlorophenyl)azo-3-hydroxy-N-phenyl-naphthalene-2-carboxamide (**3b**)*

2-Hydroxy-3-naphthoic acid anilide (2.5 g, 0.010 mol) was charged into a flask (100 ml) with NMP (24.0 g) and sodium hydroxide (0.69 g, 0.017 mol). The mixture was stirred at 40°C and then cooled below 5°C. After 2,5-dichloroaniline diazonium fluoroboric salt (2.97 g, 0.011 mol) had been added to the flask while stirring and keeping the temperature below 5°C, the solution was stirred overnight at room temperature, and neutralization using acetic acid was performed. The red powder generated was filtrated and washed sequentially with acetone, methanol and water. Finally, the powder was dispersed in methanol, filtrated, and dried in an oven at 80°C. The powder thus obtained (2.6 g, 0.005 mol) was further treated in DMF (20 g) at 120-130°C for 3 hours while stirring. The product was washed with DMF and methanol and dried in an oven at 80°C. Yellowish red 4-(2,5-dichlorophenyl)azo-3-hydroxy-N-phenyl -naphthalene-2-carboxamide (2.5 g) was obtained. Yield 60.3%; decomposition point 305°C; EI-TOF MS *m/z* 435.0538, calcd for $C_{23}H_{15}Cl_2N_3O_2$ 435.0541.

*2.4.9 Synthesis of 4-(2-methyl-5-nitrophenyl)azo-3-hydroxy-N-phenylnaphthalene-2-carboxamide (**4b**)*

2-Hydroxy-3-naphthoic acid anilide (2.5 g, 0.001 mol) was charged into a flask (100 ml) with NMP (20.0 g) and sodium hydroxide (0.84 g, 0.021 mol). The mixture was stirred at 40°C and then cooled below 5°C. After 2-methyl-5-nitroaniline diazonium fluoroboric salt (2.86g, 0.011mol) had been added to the flask while stirring and keeping the temperature below 5°C, the solution was stirred overnight at room temperature, and neutralization using acetic acid was performed. The red powder generated was filtrated and washed sequentially with acetone, methanol and water. Finally, the powder was dispersed in methanol, filtrated, and dried in an oven at 80°C. The powder thus obtained (2.6 g, 0.005 mol) was further treated in DMF (20 g) at 120-130°C for 3 hours while stirring. The product was washed with DMF and methanol and dried in an oven at 80°C. Bluish red 4-(2-methyl-5-nitrophenyl)azo-3 -hydroxy-N-phenylnaphthalene-2-carboxamide (2.5g) was obtained. Yield 61.7%; decomposition point 310°C; EI-TOF MS *m/z* 426.1335, calcd for $C_{24}H_{18}N_4O_4$ 426.1328.

2.4.10 MO and CI calculations

Semi-empirical MO calculation with the Hamiltonian, AM1, was employed in the present study, followed by singly excited configuration interaction calculations with the INDO/S method using 20 occupied and vacant orbitals. All calculations were done with SCIGRESS MO Compact (Fujitsu Ltd.). Each compound was modeled initially with the modeling software DS Modeling (Accelrys Inc.) and then by geometry optimization during the MO

calculation with AM1.

*2.4.11 Evaluation of light-fastness of **3a** to **4b***

The following materials were put in a 70 ml mayonnaise bottle: Pigment (0.12 g), zirconia beads (ϕ 0.3 mm, 3 g), solvent-soluble acrylic resin BR-87 (5.0 g), and ethyl acetate (2.4 g). The materials were mixed with a ball mill by rotating the bottle for 5 hours to disperse the pigment. The ink obtained was dropped on a slide glass and spin-coated (500 rpm) to form a transparent thin film. The films were placed in Solar Simulator HAL-320 (Xe-lamp, irradiation intensity 75mW/cm^2 (400 to 1100 nm) to be irradiated for 48 hours in air.

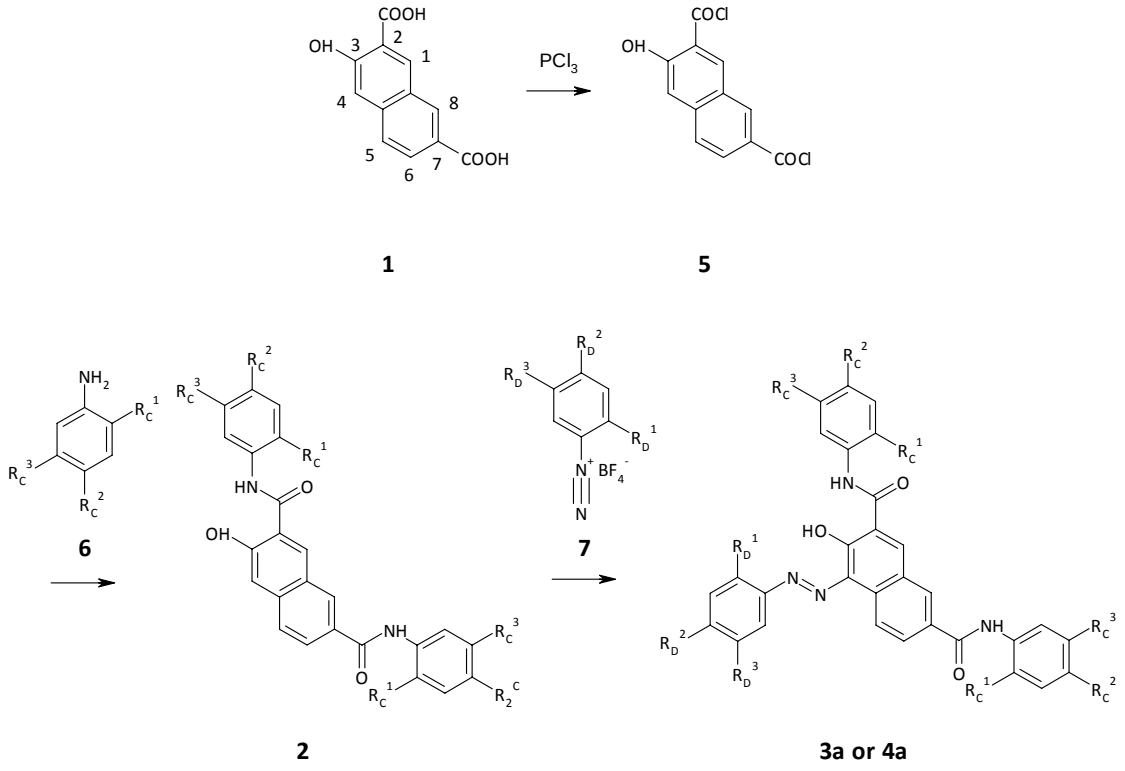

Scheme 1 Syntheses of coupling component **2** and azo pigments **3a** and **4a** starting from 3-hydroxy-2,7-naphthalene dicarboxylic acid **1**. Aniline **6**, its fluoroboric salt **7** and the pigment structure are given in a general formula. R_C^1, R_C^2 and R_C^3 on **6**, and R_D^1, R_D^2 and R_D^3 on **7** represent substituents available including hydrogen (**3a**: $R_D^1 = R_D^3 = Cl$, and $R_C^1 = R_C^2 = R_C^3 = R_D^2 = H$; and **4a**: $R_D^1 = CH_3$, $R_D^3 = NO_2$, and $R_C^1 = R_C^2 = R_C^3 = R_D^2 = H$).

2.5 Results and discussion

2.5.1 Syntheses

Conventional 7-unsubstituted azonaphtharylamide pigments are divided into two groups in terms of the number of the amide group [1]. Group 1 contains a single amide group derived from 2-naphthoic acid, and Group 2 contains one or more additional amide groups (and/or sulfonamide groups) attached to the diazo component and/or 2-phenylcarboxamide. The pigments having a 7-substituent like **3a** and **4a** are the members of neither Group 1 nor Group 2 by the above definition due to presence of a 7-subtituent. Consequently, if the pigments derived from **2** demonstrate any advantages from technological and/or industrial point of view over the conventional azonaphtharylamide pigments, those pigments will create another new subclass of azo pigments.

Syntheses of coupling component **2** and pigments **3a** and **4a** are shown in Scheme 1. In the process, 3-hydroxy-2,7-naphthalene dicarboxylic acid **1** was allowed to react with phosphorus trichloride to give acid chloride **5**, which was then amidated with aniline **6** to afford **2**. This compound was allowed to react with aniline diazonium fluoroboric salt **7** to produce **3a** or **4a**. For the synthesis, fluoroboric salt **7** was used because it is chemically stable and convenient to handle compared with the conventional chloride and nitrate salts [18]. The crude pigments were heated in N,N-dimethylformamide at 120-130°C for 3 hours to promote crystal growth [19]. The pigments thus obtained were more insoluble than the counterparts (**3b** and **4b)** in both polar and non-polar solvents. The pigments **3a** and **4a** in a powder state as obtained were yellowish and bluish red, respectively, resembling those of **3b** and **4b**.

It is important to underline that the 7-position of diacid **1** can be selectively esterified in contrast to the 2-position. This selectivity is attributed to the fact that the HOMO of the diacid, as shown in Figure. 2 (A), extends its lobe on the 7-carbonyl's oxygen atom, which attracts a proton from an acid catalyst; the HOMO does not extend on the 2-carbonyl's oxygen atom. When the 7-carbonyl is protonated, as shown in Figure 2 (B), the LUMO of the protonated diacid has the prominent lobe on the 7-carbonyl's carbon atom, which will be nucleophilically attacked by the oxygen atom of an alcohol. It is thus possible to introduce two mutually different functional groups into the 2- and 7-positions by dividing the amidation process into two steps (Scheme 2). The 7-carboxylic acid on **1** is first protected by an appropriate esterification to yield monoester **8** and then chloridized. Acid chloride **9** is 2-amidated with aniline derivative **10** in the first amidation step. Amidated ester **11** is then hydrolyzed (**12**) and subsequently chloridized. Acid chloride **13** is then 7-amidated with another aniline derivative **14**. The above sequence will definitely facilitate extensive derivatization for a large variety of coupler structure **15**. This has been in fact substantiated in a reference [**20**].

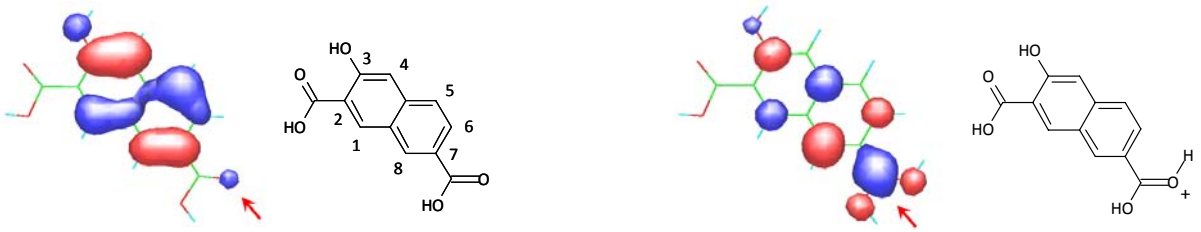

(A) HOMO (B) LUMO of the protonated product

Figure 2 MOs to demonstrate selective esterification at 7-carboxylic acid of **4**. The corresponding chemical structures are shown on the right side of each MO. (A) depicts the HOMO, indicating the lobe of the carbonyl's oxygen atom to be protonated by an acid catalyst, and (B) the LUMO of 7-protonated **4**, exhibiting electrophilicity of the carbonyl's carbon atom, as emphasized by the red arrows.

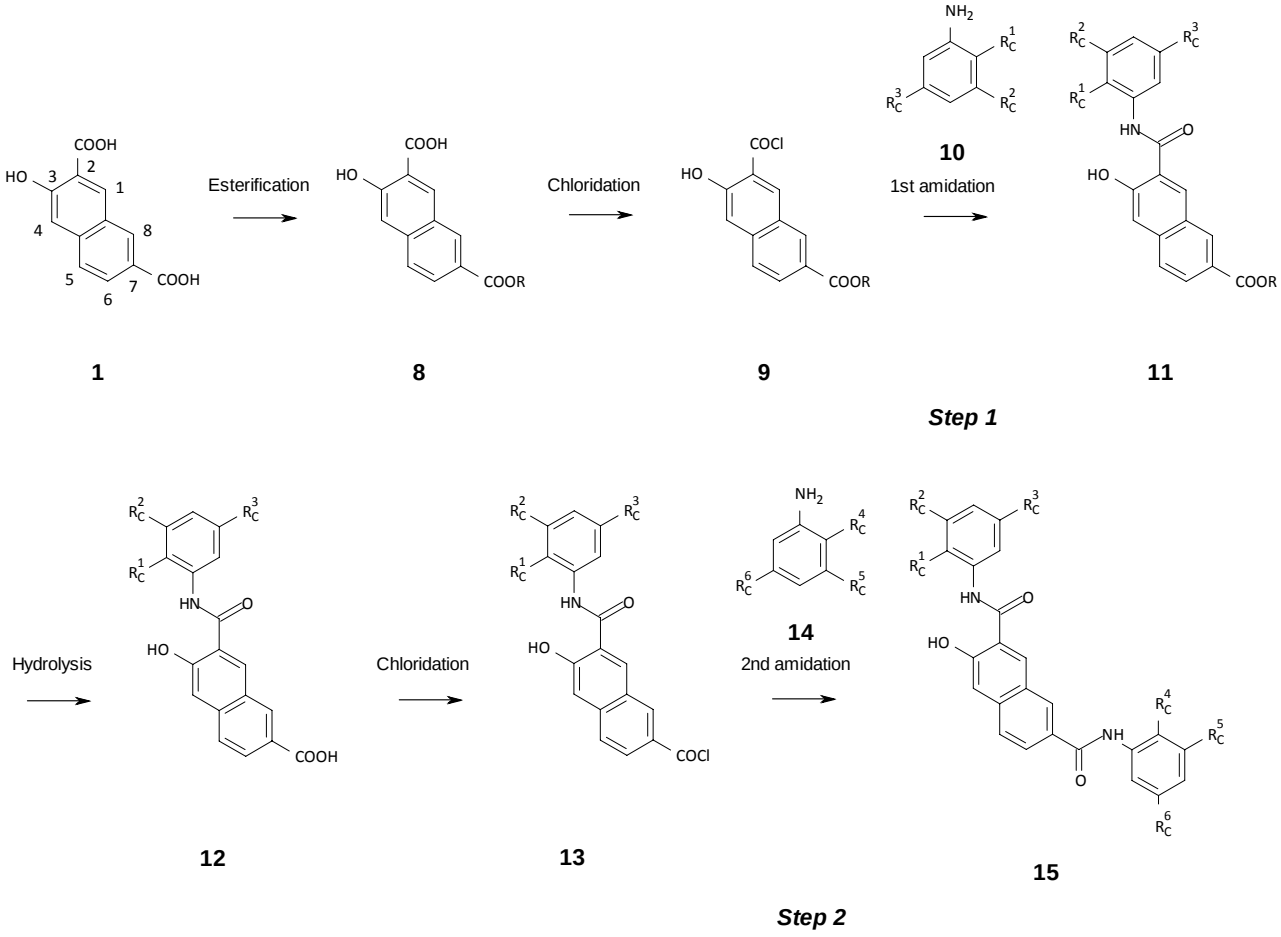

Scheme 2 Introduction of mutually different substituents to 2- and 7-positions of **1**. The amidation sequence is divided into the two steps utilizing selective esterification of 7-position of **1**. Anilines **10** and **14** are given in a general formula. R_C^1 to R_C^6 on **10** and **14** indicate the substituents available including hydrogen.

*2.5.2 Crystallinity of **3a** and **4a***

Powder X-ray diffraction patterns of **3a** and **4a** are shown in Figures 3 and 4, respectively, together with those of **3b** and **4b**. Although they were heat-processed for crystal growth as mentioned above, the diffraction bands of **3a** and **4a** are broader than those of **3b** and **4b**.

The sizes of the crystallites of **3a** and **4a** were estimated to be 14.8 and 8.8 nm, respectively, using Scherrer equation from the half maxima of the diffraction peaks at around 2θ = 27.5°. Similarly, the sizes of the crystallites of **3b** and **4b** were estimated to be 16.1 and 16.0 nm, respectively. These results may suggest that the 7-phenylcarboxamide substituent hindered the growth of the crystallites of **3a** and **4a**.

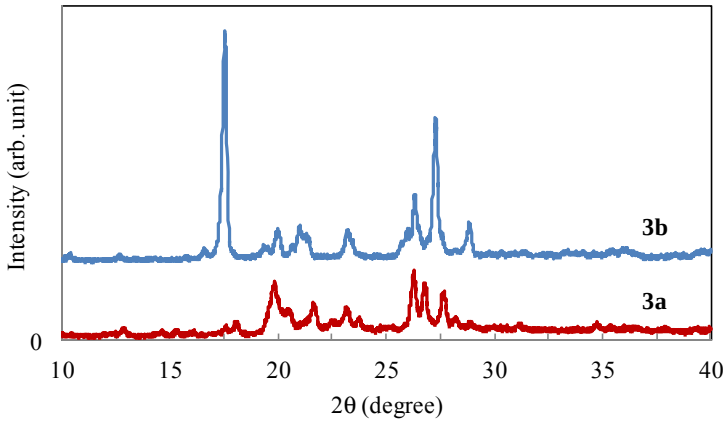

Figure 3 X-ray diffraction patterns of **3a** and **3b** which were heat-processed at 120-130°C in N,N-dimethylformamide for 3 hours for crystal growth promotion.

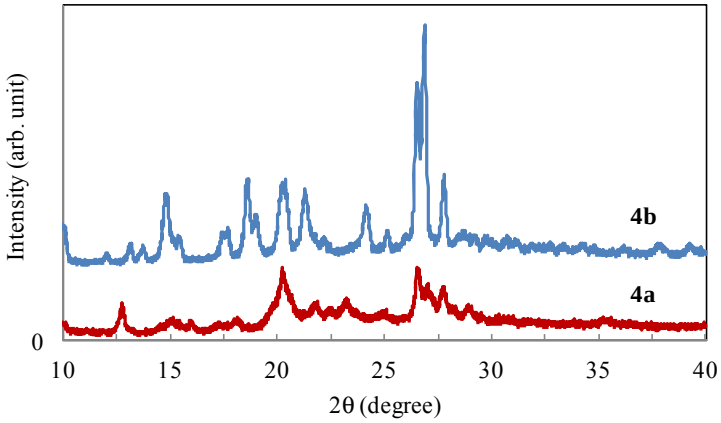

Figure 4 X-ray diffraction patterns of **4a** and **4b** which were heat-processed at 120-130°C in N,N-dimethylformamide for 3 hours for crystal growth promotion.

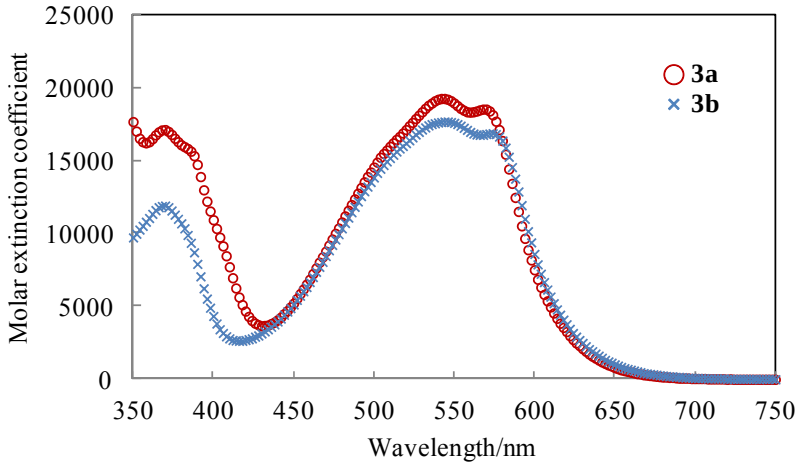

Figure 5 Optical absorption spectra of **3a** and **3b** in N-methylpyrrolidone.

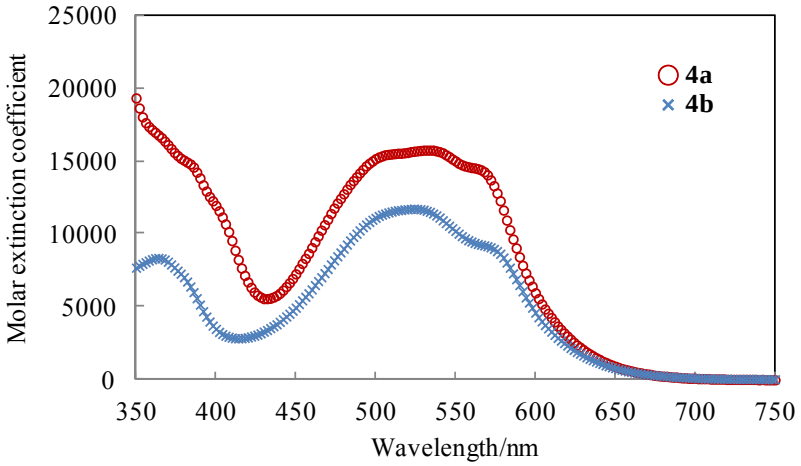

Figure 6 Optical absorption spectra of **4a** and **4b** in N-methylpyrrolidone.

Table 1 Wavelengths of optical absorption maxima and molar extinction coefficients of **3a** and **3b** in N-methylpyrrolidone.

λ_{max}^{abs}/nm		ε_{max}/dm^3 mol^{-1} cm^{-1}	
3a	**3b**	**3a**	**3b**
569	574	18500	16900
543	545	19200	17600
[a]498sh	[a]508sh	15000	14900
[a]387sh	[a]380sh	15500	16700
370	368	17100	11900

[a] sh: shoulder absorption.

Table 2 Wavelengths of optical absorption maxima and molar extinction coefficients of **4a** and **4b** in N-methylpyrrolidone.

λ_{max}^{abs}/nm		ε_{max}/dm^3 mol^{-1} cm^{-1}	
4a	**4b**	**4a**	**4b**
[a]569sh	[a]578sh	14100	8600
533	524	15700	11700
[a]501sh	[a]498sh	15200	10900
[a]407sh	[a]382sh	10400	6700
389sh	364	14000	8300

[a] sh: shoulder absorption.

2.5.3 UV-Vis absorption spectra of the pigments

Figures 5 and 6 show UV-Vis optical absorption spectra of **3a** and **3b** and of **4a** and **4b**, respectively, in N-methylpyrrolidone. The four compounds exhibit two broad and almost structureless bands: One from 470 to 580 nm and the other from 350 to 400 nm. Tables 1 and 2 summarize wavelengths of the absorption maxima and molar extinction coefficients of **3a** and **4a**, respectively, together with those of **3b** and **4b**. A bathochromic shift was not observed between **3a** and **3b** or between **4a** and **4b**. A hyperchromic effect of **3a** and **4a** was, however, clearly observed, particularly in the shorter wavelength region. The absence of a bathochromic shift suggests that extent of the chromophore systems of **3a** and **4a** are comparable with those of **3b** and **4b**, respectively, and that there is little involvement of the 7-substituent in the chromophore systems. This is consistent with the similarity of color tones in the powder samples. The hyperchromic effect observed will be discussed later.

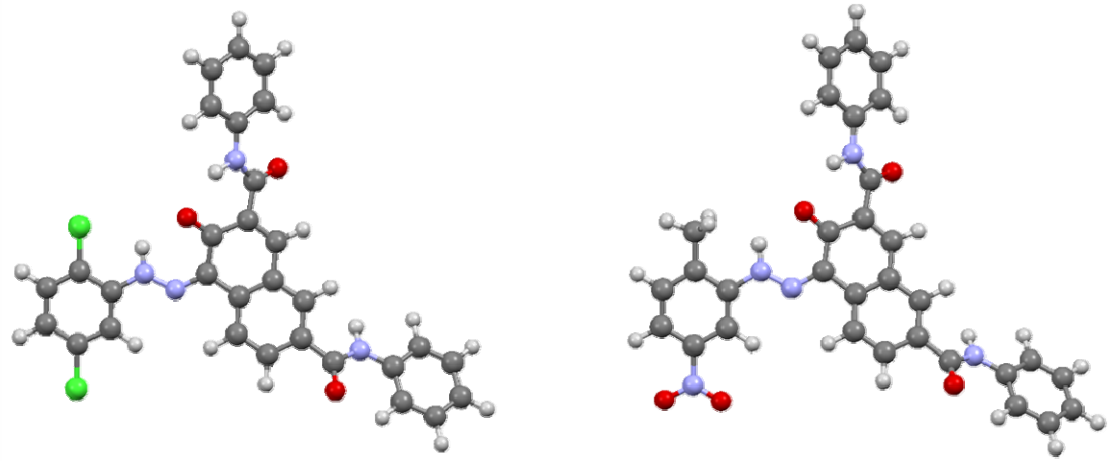

3a **4a**

Figure 7 Optimized molecular geometries of **3a** and **4a** having keto-hydrazone configurations.

2.5.4 MO calculations for molecular geometry and electron transition

It has been shown that azonaphtharylamide pigments tend to adopt a keto-hydrazone form in solution and crystalline states [19,21,22]. A study on 1-phenylazo-2-naphthols also showed that the ketohydrazone form is energetically more stable than the hydroxyazo form based on results of crystal structure analyses and DFT calculations [23]. Therefore, the molecular geometry of **3a** and **4a** was optimized with a keto-hydrazone configuration using modeling software and by a semi-empirical molecular orbital (MO) calculation method. Figure 7 shows the optimized geometries, and Table 3 summarizes the dihedral angles between the least square planes of the naphthalene ring and the phenyl ring of the 2-, 4- or 7-position, where the dihedral angles were calculated by using the atomic coordinates obtained through the

geometry optimization. Table 3 includes also the dihedral angles of those in **3b** and **4b** of the optimized structures with a keto-hydrazone configuration through the same calculation manner for comparison. These results indicate that both of the two phenyl rings attached to the naphthalene ring via the carboxamide groups are twisted relative to the naphthalene plane, while the phenyl ring attached to the naphthalene ring via the hydrazone group is less twisted to the naphthalene ring. The twist at the 2-position is more or less small compared with that at the 7-position in **3a** and **4a**.

Table 3 Dihedral angles between the least square planes of the naphthalene ring and the phenyl rings of **3a**, **3b**, **4a** and **4b**. The least square planes were calculated by using the atomic coordinates obtained in the geometry optimization.

Position of a phenyl substituent (on a naphthalene ring)	Dihedral angle vs. naphthalene (degree)			
	3a	**3b**	**4a**	**4b**
4	17.5	15.9	21.1	14.0
2	29.4	27.6	28.0	27.2
7	30.3	–	31.2	–

Table 4 Optical absorption spectra of **3a** and **4a** in the ketohydrazone-form calculated by the semi-empirical MO method and their band positions experimentally observed in N-methylpyrrolidone.

Compound	**Absorption [nm]**	**Oscillator strength**	**CI component**[a]			**Absorption band in N-methylpyrrolidone [nm]**
3a	417.0	0.6034	HOMO	→	LUMO (58%)	470-580
	353.7	0.2037	HOMO-3	→	LUMO (36%)	
	310.8	0.2504	HOMO	→	LUMO+1 (22%)	
			HOMO-3	→	LUMO+1 (15%)	
	280.5	0.4110	HOMO-2	→	LUMO (27%)	350-400
	268.6	0.4759	HOMO	→	LUMO+1 (15%)	
			HOMO	→	LUMO+2 (15%)	
			HOMO-2	→	LUMO (11%)	
4a	414.0	0.5962	HOMO-1	→	LUMO (50%)	470-580
	355.4	0.2283	HOMO-3	→	LUMO (47%)	
	309.7	0.2262	HOMO-6	→	LUMO (17%)	
			HOMO-1	→	LUMO+2 (17%)	
	285.6	0.1256	HOMO-2	→	LUMO (52%)	350-400
	270.7	0.3100	HOMO-1	→	LUMO+2 (25%)	
	269.3	0.4977	HOMO	→	LUMO+3 (25%)	

[a] Percentages of CI (configuration interaction) components are shown in brackets.

The above geometry supports the possibility that the π-conjugation or chromophore system of **2a** and **3a** is analogous to that of **3b** and **4b**, and is constituted substantially with the naphthol ring, 2-phenylcarboxamide and 4-phenylhydrazone. Involvement of 7-phenylcarboxamide in the chromophore systems of **3a** and **4a** should be therefore much less compared with that of 2-phenylcarboxamide. If **3a** and **4a** form molecular crystals with no strong intermolecular interaction like other azonaphtharylamide pigments [19,21-26], their color properties originate in their isolated molecular structures and should be similar to those in solutions. The above chromophoric analogy should be responsible for the resemblance in the contours of the optical absorption spectra between **3a** and **3b** and between **4a** and **4b**.

The longest wavelength bands of **3a** and **4a** calculated by the semi-empirical MO method are summarized in Table 4. They appeared in higher energy regions than those of the experimentally observed bands. Such shifts toward higher energy regions are generally observed in semi-empirical calculations [27,28]. The computations indicate that the longest wavelength bands for **3a** and **4a** are due to π-π* transitions from the HOMO or orbitals close to it to the LUMO or orbitals close to it. The molecular orbitals involved in the transitions are shown in Figures 8 and 9 for **3a** and **4a**, respectively. These figures illustrate that the following orbitals contain electron localization on the 7-phenylcarboxamide group: (**3a**) HOMO-2, LUMO+1 and LUMO+2, and (**4a**) HOMO-2, HOMO-1, LUMO+2 and LUMO+3. Therefore, although the 7-substituent hardly contributes to extension of the chromophore system, the electron localization on the 7-substituent surely contributes to increment of transition probability, inducing the hyperchromic effect as observed with **3a** and **4a**.

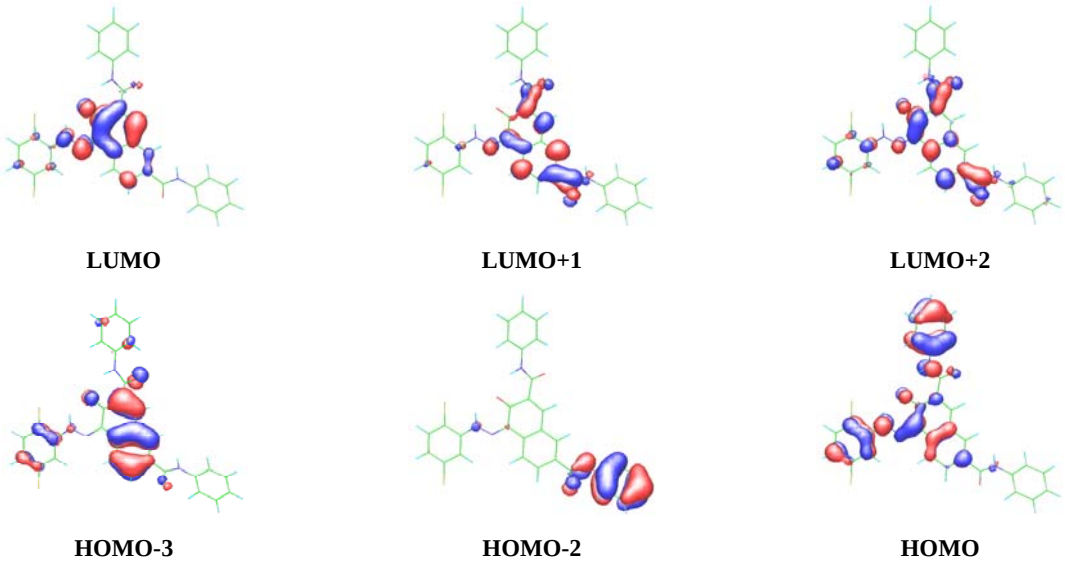

Figure 8 Molecular orbitals of **3a** (keto-hydrazone form) involved in the transitions for longest wavelengths (see Table 4 also).

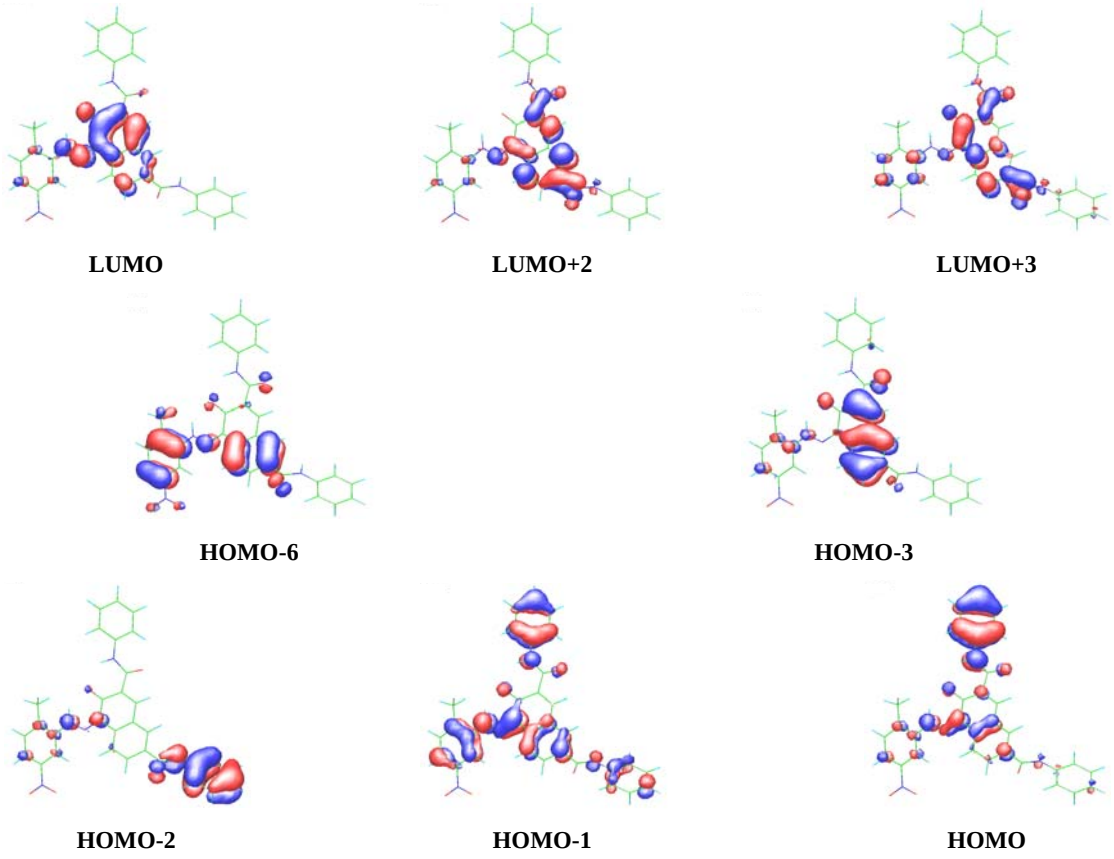

Figure 9 Molecular orbitals of **4a** (keto-hydrazone form) involved in the transitions for longest wavelengths (see Table 4 also).

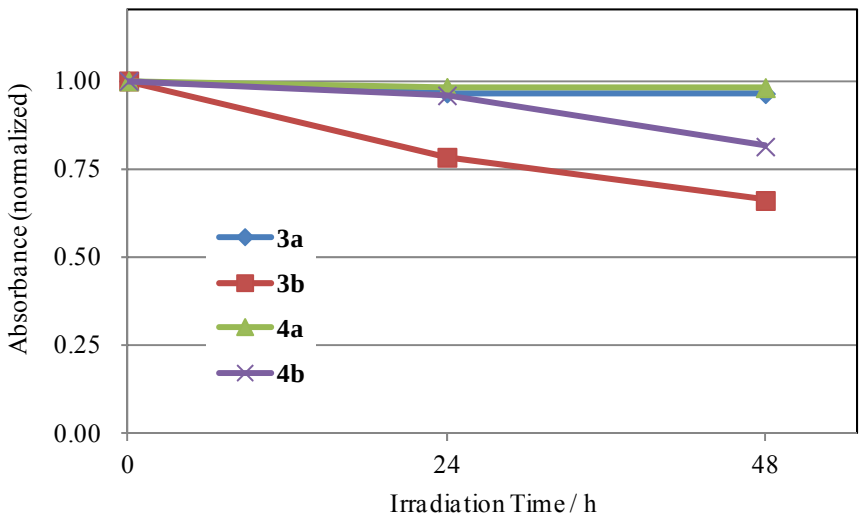

Figure 10 Light fastness of **3a**, **3b**, **4a** and **4b**. The pigments were dispersed in acrylic films and irradiated with a Xe-lamp (75 mW/cm^2; 400 to 1100 nm). For each sample, the absorbance at the peak absorption wavelength is plotted for irradiation periods of 24 and 48 h. The absorbance is normalized by the absorbance of the sample before photoirradiation.

*2.5.5 Light-fastness of **3a** and **4a***

The durability of organic pigments, both azo and heterocyclic pigments, has been discussed in relation to intramolecular and/or intermolecular interactions, including hydrogen bonding, π-π stacking, and van der Waals contact. A strong intermolecular hydrogen bond binds diketopyrrolopyrrole or quinacridone molecules in their crystal structures, which is one of the important factors for imparting durability to these pigments [29,30]. Concerning conventional 7-unsubstituted azonaphtharylamide pigments, no strong intermolecular hydrogen bond network has been found. Alternatively, stabilization of the bifurcated intramolecular hydrogen bonds formed among the keto-hydrazone and 2-carboxamide groups has been proposed to explain the durability [19,21]. It has also been pointed out that increase in the number of amide groups tends to improve the technical performance of the azonaphtharylamide pigments, e.g., resistance to light, heat, solvent and/or migration [1,19,21], as experimentally demonstrated for the aforementioned Group 2 pigments.

Since **3a** and **4a** possess the two amide groups, these pigments are expected to outperform in durability **3b** and **4b,** which belong to conventional Group 1 pigments. It was therefore interesting to evaluate light fastness of **3a**, **3b**, **4a**, and **4b**. The pigments were dispersed in transparent films of an acrylic resin. Changes in the absorption spectra of the films in the visible light region were monitored while they were photo-irradiated at the intensity of 75 mW/cm^2 (400 to 1100 nm) for 48 hours using a Xe lamp as the light source. Figure 10 shows the changes in the absorbance of the films at their absorption maxima. The maxima of the films at time 0 are normalized to unity in Figure 10. The results show that **3a** and **4a** have higher light fastness than **3b** and **4b**, as expected from the discussion on the number of the amide groups. Improved chemical stability of the pigments will also enhance their heat resistivity. This tendency was confirmed by the increase in the decomposition points of **3a** and **4a** compared with those of **3b** and **4b**, as shown in Table 5.

Table 5 Decomposition points of **3a**, **3b**, **4a** and **4b** evaluated by TG/DTA.

Compound	**3a**	**3b**	**4a**	**4b**
Decomposition point (°C)	339	305	320	310

2.6 Conclusion

Effect of a 7-substituent of two7-substituted azonaphtharylamide pigments was studied. The pigments were obtained using the coupling component, 3-hydroxy-N2,N7-diphenyl -naphthalene-2,7-dicarboxamide, derived from 3-hydroxy-2,7-naphthalene dicarboxylic acid.

Presence of 7-phenycarboxamide distinguishes the pigments from conventional azonaphtharylamide pigments derived from 3-hydroxy-2-naphthoic acid. The 7-substituted pigments exhibited higher insolubility, higher decomposition points, and relatively lower crystallinity than those of the 7-unsubstituted counterparts. The optical absorption spectra of the 7-substituted pigments in solution showed a hyperchromic effect and did not show a bathochromic shift compared with the 7-unsubstituted counterparts. Molecular geometry optimizations through semi-empirical MO calculations showed that extent of the chromophore system of the 7-substituted pigments is comparable with those of the counterparts, accounting for absence of the bathochromic shit. The calculations elucidated the hyperchromic effect, which is provided by involvement of the 7-substituent in the electronic transitions in the longest wavelength bands. The 7-substituted pigments demonstrated durability superior to that of the 7-unsubstituted ones. Consequently, the 7-substituted pigments are expected to create a new subclass of azonaphtharylamide pigments.

Chapter 3

Synthesis and Structure Determination from Powder X-ray Diffraction Data of Black Azo (Hydrazone) Pigments

3.1 Abstract

Two novel black azo (hydrazone) pigments were synthesized starting from 3-hydroxy-2-naphthoic acid and 3-hydroxy-2,7-naphthalene dicarboxylic acid. The crystal structures of the pigments have been determined from powder X-ray diffraction data combined with DFT calculations. The DFT calculations suggested the molecules are in hydrazone forms but not in azo forms in both crystal structures. The two molecules are highly planar yielding a large π conjugation or chromophore system which allows the molecules to have a wide variety of electron transitions in the visible light range with a bathochromic shift. The arrangements of the transition dipoles in the crystal structures suggested that the Davydov splitting may occur by the excitonic interactions and it causes also the red absorption band shift in the crystalline state leading the characteristic black colors.

3.2 Introduction

Carbon black (CB) is industrially one of the most popular and important products as a black shade pigment. CB is inexpensive and useful boasting of its outstanding durability in various applications such as colorant for paints, printing inks and plastics, as well as a reinforcing component for rubber. CB has been applied also for liquid crystal display (LCD) panels as colorant for the black matrix which is indispensable to separate the color filter pixels of the three primary colors of light, i.e., red, green and blue, equipped on thin-film transistors. It has been, however, pointed out that benzpyrene and other impurities, which are the byproducts generated through the production processes of CB, can be carcinogenic and are unavoidably contained in CB for commercial products. Electric conductivity of CB has been another issue in the application for LCD panels, whereas electric insulation of the black matrix is required to ensure action performance of the transistors. There is therefore a demand for a new black pigment which can replace carbon black [31]. In this chapter, novel black azo pigments using naphthol couplers are discussed based on the conclusion of Chapter 2.

Broad optical absorption bands in the visible wavelength region are necessary to

obtain black color. In case of organic aromatic materials, extension of a π-conjugation system provides: (1) Narrowing of the HOMO-LUMO gap (red shift of the optical absorption), and (2) increment of bonding and anti-bonding molecular orbitals, thereby hopefully inducing various electronic transitions between numbers of those molecular orbitals. The extension would be therefore useful for a strategy to design a black pigment.

In Chapter 2, two new red azonaphtharylamide pigments were studied, where the pigments possess phenyl groups at 2- and 7-positions of the naphthol ring connected via the secondary amide bridges. As a consequence of the discussion, it was concluded that the sizes of the chromophore of the pigments are almost equivalent to those of the conventional 7-unsubstituted counterparts and the 7-substituent can hardly join in the chromophore or π-conjugation system, while the 7-substituent can correlate to the electron transitions of the pigments. In conventional azonaphtharylamide pigments, i.e., 7-unsubstituted azonaphtharylamide ones, the secondary amide bridge binds the naphthol with 2-substituent. The amide bridge includes the nitrogen atom having the sp3 hybrid orbit, which fundamentally tends to form a tetrahedral structure. Crystal structure analyses for some conventional azonaphtharylamide pigments, however, have revealed that the nitrogen atom exists in a highly planar state, constituting a part of the π-conjugation system of a keto-hydrazone configuration [19,21,22,24]. In contrast, it is suggested that a tetrahedral structure or its modification derived from the sp3 nitrogen atom would be more or less preserved in the amide bridge at the 7-position leading poor planarity. Consequently, secondary amide is inconvenient for the 7-position to obtain black hue through extending the π-conjugation system. Alternatively, carbon-carbon bridge, for example, would be better than secondary amide to directly bind the naphthol with 7-substituent in extension of the π-conjugation system, although potential for rotation or torsion between them would remain.

Let us then discuss a substituent to be introduced on naphthol for materializing black color. Pigments belonging to the subclasses of azonaphtharylamide or benzimidazolone typically have unsubstituted or substituted phenyl group for the diazo component and unsubstituted or substituted phenyl or benzimidazolone group for the coupling components (naphthol). Those pigments exhibit mostly red, orange and brown to yellow hues, suggesting that black is unattainable as far as phenyl and benzimidazolone groups are used. On the other hand, benzothiazole have been employed in some azo disperse dyes [32]. Some of the dyes containing mono-substituted benzothiazole can be more bathochromic than their carbocyclic analogs [33]. Even smaller thiazole can be used for dark colored azo dyes [34]. These

results suggest that thiazole analogs are useful for a substituent of black pigments, although the above heteroaromatics were used for the diazo components. Naphthothiazole is larger than benzothiazole in size, and will be further interesting as a thiazole analog.

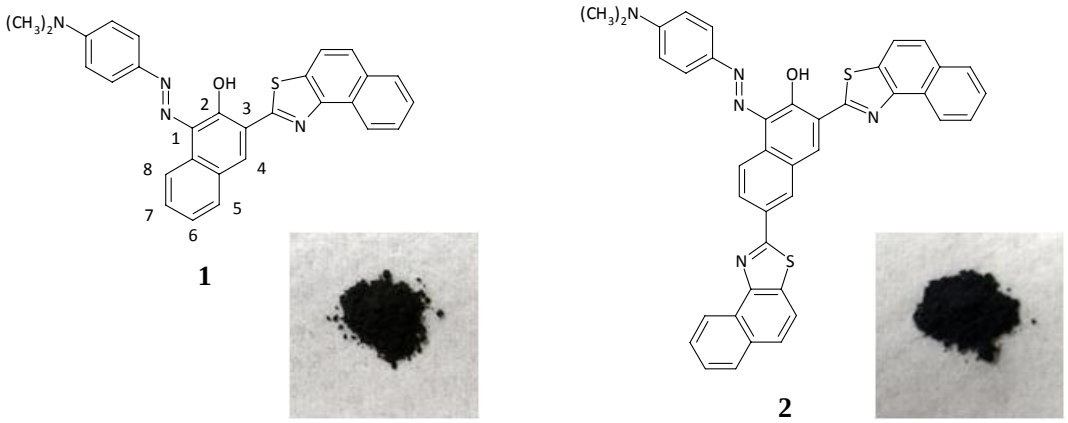

Figure 1 Molecular structures of two black azo pigments: 1-(4-dimethyl-amino-phenylazo)-3-naphtho[1,2-d]thiazol-2-yl-naphthalen-2-ol (**1**) and 1-(4-dimethyl-amino-phenylazo)-3,6-bis-naphtho[1,2-d]thiazol-2-yl-naphthalen-2-ol (**2**). Appearance of the compound is shown as the picture placed in lower right of each chemical structure. The structures of **1** and **2** are depicted in the hydroxy-azo configurations, although they are believed to have the keto-hydrazone configurations.

In this chapter, an attempt has been made (Figure 1) to prepare two novel black azo pigments, 1-(4-dimethyl- amino-phenylazo)-3-naphtho[1,2-d]thiazol-2-yl-naphthalen-2-ol (**1**) and 1-(4-dimethyl- amino-phenylazo)-3,6-bis-naphtho[1,2-d]thiazol-2-yl-naphthalen-2-ol (**2**), without using amide linkages, i.e., preparation of non-azonaphtharylamide-type pigments. Azonaphtharylamide pigments usually show red to yellow colors, and characteristic black colors of the above compounds would be due to their broadly extended π-conjugation systems as expected. In order to confirm this point, crystal structure analysis for the compounds is a powerful tool to elucidate extension of the π-conjugation systems, i.e., co-planarity between the naphthol and naphthothiazole rings. However, unfortunately, preparation of single crystals of these compounds has remained unsuccessful because of their low solubility and no sublimation property, and their crystal structures have been left to be unsolved. In such case, techniques for carrying out structure determination directly from powder X-ray diffraction data (ab initio PXRD analysis) are clearly essential to reveal crystal structures without preparation of single crystals. Ab initio PXRD analysis for organic

molecular materials has been developed in recent years [35-37]. This chapter presents the crystal structures of **1** and **2** which have been determined by ab initio PXRD analysis combined with density functional theory (DFT) calculation.

3.3 Experimental

3.3.1 Materials

All the chemicals were purchased from Tokyo Kasei Co., Ltd. except 3-hydroxy-2,7-naphthalene dicarboxylic acid. The above diacid was purchased from Wako Pure Chemical Industries.

3.3.2 Instruments

UV-Vis absorption spectra in solution and in solid (powder) were measured with HITACHI U-3310 Spectrophotometer and JASCO V-560 Spectrophotometer, respectively. Mass spectra were taken on Waters Alliance-ZMD LC/MS Spectrometers to identify each intermediate. Mass spectra and elemental analyses for **1** and **2** were taken on JEOL JMS-700 (EI-TOF MS) and Elementar Analytical elemental analyzer vario MICRO cube, respectively. Thermogravimetric analysis (TGA) and differential thermal analysis (DTA) were performed on a Rigaku Thermo Plus 2. IR spectra of **1** and **2** were taken on Bio-Rad Laboratories, Excalibur FTS 3000 FTIR-Spectrophotometer.

3.3.3 Synthesis of 1-amino-naphthalene-2-thiol

The synthesis was performed according to the procedures described in a reference [38]. Thionyl chloride (60ml) was charged in a flask (500 ml). 1-(1-Naphthyl)-2 -thioulea (14.5 g, 0.07 mol) was added in the flask keeping the mixture at 30-40°C. Additional 30 ml of thionyl chloride was then added. The mixture was stirred at 50-55°C for 1.5 hours. After cooling to room temperature, ethyl acetate (100 ml) was poured into the flask, followed by filtration. The resulting precipitates were dried under reduced pressure to yield naphtho[1,2-d]thiazol-2-yl-amine (14.0 g) almost stoichiometrically as white powder. m/z(-)=201, calcd for $C_{11}H_8N_2S$ 200.26.

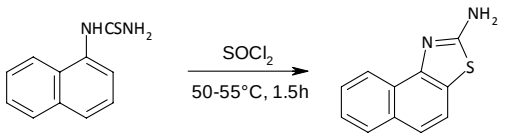

The following materials were charged in a flask (500 ml): 98% Sodium hydroxide (20 g, 0.5 mol), ethylene glycol (90 ml) and water (20 ml). Naphtho[1,2-d]thiazol -2-yl-amine (9.0 g, 0.045 mol) was added in the flask and the mixture was refluxed under N_2 gas flow for 20 hours. The solution was diluted with water (50 ml) and cooled to room temperature. Extraction using diethyl ether (50 ml) was applied for three times to remove the starting materials, and the aqueous fraction was neutralized with acetic acid. The aqueous suspension was again extracted using diethyl ether (90 ml) for three times. The resulting ether layer was washed with water, and dried with magnesium sulfate. After removal of the sulfate, ether was distilled out under reduced pressure to yield 1-amino-naphthalene-2-thiol (5.5 g) as yellow powder (yield 69.9%). m/z(-)=174, calcd for $C_{10}H_9NS$ 175.25.

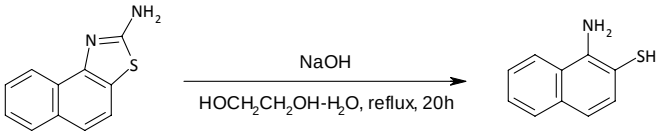

3.3.4 Synthesis of 3-naphtho[1,2-d]thiazol-2-yl-naphthalen-2-ol

The following substances were charged in a flask (500 ml): 3-Hydroxy-2-naphthoic acid (5.0 g, 0.027 mol), 1-amino-naphthalene-2-thiol (5.5 g, 0.031 mol), phosphorous trichloride (4.4 g, 0.032 mol) and sulfolane (30 g). The mixture was heated to 140°C and stirred for 3 hours, then cooled to room temperature. After filtration, the precipitates were washed with methanol, followed by dry to yield 3-naphtho[1,2-d]thiazol-2-yl –naphthalen-2-ol (5.7 g) as yellow powder (yield 65.3%). m/z(+)=328, m/z(-)=326, calcd for $C_{21}H_{13}NOS$ 327.40.

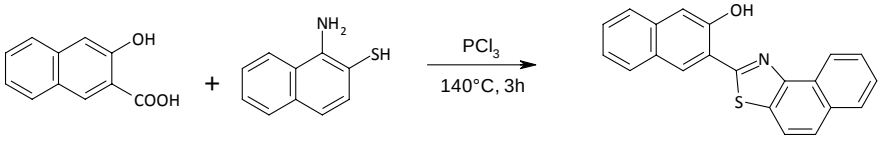

3.3.5 Synthesis of 3,6-bis-naphtho[1,2-d]thiazol-2-yl-naphthalen-2-ol

The following substances were charged in a flask (1000 ml): 3-Hydroxy -2,7-naphthalene dicarboxylic acid (5.0 g, 0.022 mol), 1-amino-naphthalene-2-thiol (8.0g, 0.046 mol), phosphorous trichloride (5.9g, 0.043 mol) and sulfolane (110 g). The

mixture was heated to 140°C and stirred for 3 hours, then cooled to room temperature. Methanol was added and the reaction mixture was filtrated. The precipitates were put in methanol and washed, followed by sequentially filtration, a wash with N-methyl-2-pyrrolidone, filtration, and dry in an oven at 80°C to yield 3,6-bis-naphtho[1,2-d]thiazol-2-yl-naphthalen-2-ol (4.1 g) as yellow powder (yield 37.3%). m/z(-)=509, calcd for $C_{32}H1_8N_2OS_2$ 510.63.

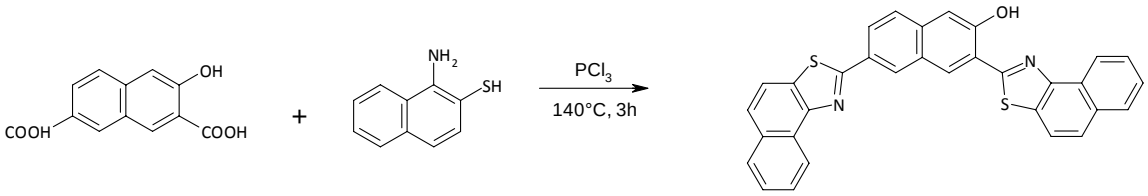

3.3.6 Synthesis of 1-(4-dimethylamino-phenylazo)-3-naphtho[1,2-d]thiazol-2-yl -naphthalen-2-ol ***(1)***

3-Naphtho[1,2-d]thiazol-2-yl-naphthalen-2-ol (2.5 g, 0.008 mol) was charged in a flask (500 ml) with N-methyl-2-pyrrolidone (20 g) and sodium hydroxide (0.7 g, 0.017 mol). The ingredients were stirred at 45°C, and then cooled below 8°C. 4-Diazo-N,N-dimethylanilinechloride zinc chloride salt (2.9 g, 0.009 mol) was added in the flask while stirring. The stir was done for 12 hours to room temperature. Acetic acid (1.1 g, 0.018 mol) was dripped for 2 hours and filtrated. The precipitates were washed using small amount of N-methyl-2-pyrrolidone then acetone, followed by wash sequentially in acetone, methanol, aqueous methanol and filtration. Finally the black powder was dispersed in methanol, filtrated and dried in an oven at 80°C. The powder thus obtained (2.6 g, 0.005 mol) was further treated in DMF (20g) at 120°C for 3 hours while stirring for crystal growth. The product was washed with DMF and subsequently methanol, and dried in an oven at 80°C to yield 1-(4-dimethylamino-phenylazo)-3 -naphtho[1,2-d]thiazol-2-yl-naphthalen-2-ol.Yield 2.2 g (61.1%). IR (KBr disk): 3055, 3028, 2980, 2913, 2858, 2802, 1684, 1602, 1552, 1526, 1521, 1506, 1483, 1467, 1440, 1413, 1369, 1338, 1330, 1284, 1272, 1232, 1214, 1200, 1176, 1165, 1147, 1125, 1081, 1069, 1023, 985, 948, 910, 876 cm^{-1}. Anal. Calcd for $C_{29}H_{22}N_4OS$: C 73.39, H 4.67, N 11.81, S 6.76 %; Found C 72.89, H 4.69, N 11.76, S 6.54 %. MS (ESI) m/z 474.1514 ([M+H]+ calcd for $C_{29}H_{22}N_4OS$: 474.1524).

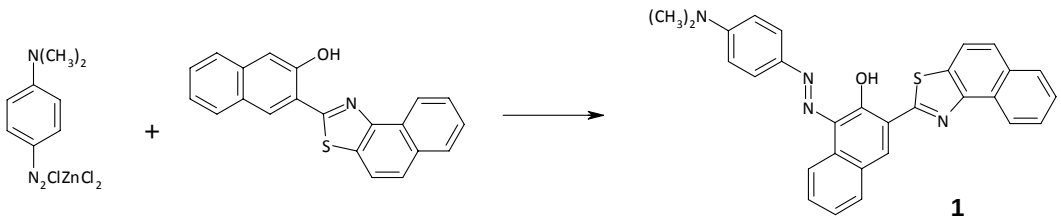

1

3.3.7 Synthesis of 1-(4-dimethylamino-phenylazo)-3,6-bis-naphtho[1,2-d]thiazol-2-yl -naphthalen-2-ol (2)

3,6-Bis-naphtho[1,2-d]thiazol-2-yl-naphthalen-2-ol (2.5 g, 0.005 mol) was charged in a flask (500 ml) with N-methyl-2-pyrrolidone (20 g) and sodium hydroxide (0.4 g, 0.010 mol). The ingredients were stirred at 45°C, and then cooled below 8°C. 4-Diazo-N,N-dimethylanilinechloride zinc chloride salt (2.9 g, 0.009 mol) was added in the flask while stirring. The stir was done for 12 hours to room temperature. Acetic acid (0.7 g, 0.012 mol) was dripped for 2 hours and filtrated. The precipitates were washed using small amount of N-methyl-2-pyrrolidone then acetone, followed by wash sequentially in acetone, methanol, aqueous methanol and filtration. Finally the black powder was dispersed in methanol, filtrated and dried in an oven at 80°C. The powder thus obtained (2.5 g, 0.004 mol) was further treated in N-methyl-2-pyrrolidone (20 g) at 120°C for 3 hours while stirring for crystal growth. The product was washed in DMF and subsequently methanol, and dried in an oven at 80°C to yield 1-(4-dimethylamino -phenylazo)-3,6-bis-naphtho[1,2-d]thiazol-2-yl-naphthalen-2-ol. Yield 2.2 g (68.8%). IR (KBr disk): 3047, 2990, 2909, 2857, 2802, 1604, 1551, 1520, 1511, 1475, 1458, 1442, 1438, 1410, 1395, 1368, 1337, 1316, 1287, 1279, 1270, 1245, 1235, 1210, 1174, 1149, 1125, 1080, 1065, 1023, 1004, 985, 947, 903, 864, 839 cm^{-1}. Anal. Calcd for $C_{40}H_{27}N_5OS_2$: C 73.04, H 4.14, N 10.65, S 9.75 %; Found C 72.90, H 4.51, N 10.18, S 9.15 %. MS (ESI) m/z 657.0719 ($[M+H]^+$ calcd for $C_{40}H_{27}N_5OS_2$: 657.1657).

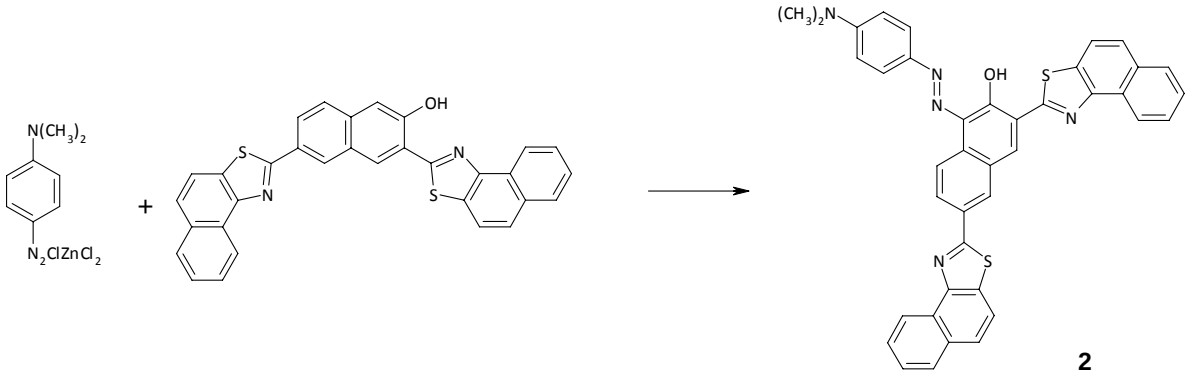

2

3.3.8 X-ray powder diffraction

Synchrotron X-ray powder diffraction data of black powdery products of **1** and **2** were recorded under ambient conditions on beamline 4B2 (Multiple Detector System) at the Photon Factory, Tsukuba, Japan, with a wavelength of 1.196734(3) Å. The samples were introduced into 2 mm diameter borosilicate glass capillaries and were used for the measurements. The data collection time was 7 hours.

Indexing of the powder X-ray diffraction data was carried out using the program X-cell [39] for **1** and DICVOL04 [40] for **2**. The structure solution calculations were carried out using the program DASH [41] followed by the Rietveld structural refinement [42] by the GSAS [43] program. In the structural refinement, standard restraints were applied to the bond lengths and bond angles, and a global isotropic displacement parameter was used.

3.3.9 DFT calculation

DFT calculations (B3LYP with a 6-31G* basis set) were carried out using the program SPARTAN'08 (Wavefunction, Inc.) to estimate energy difference of molecular structures to be discussed.

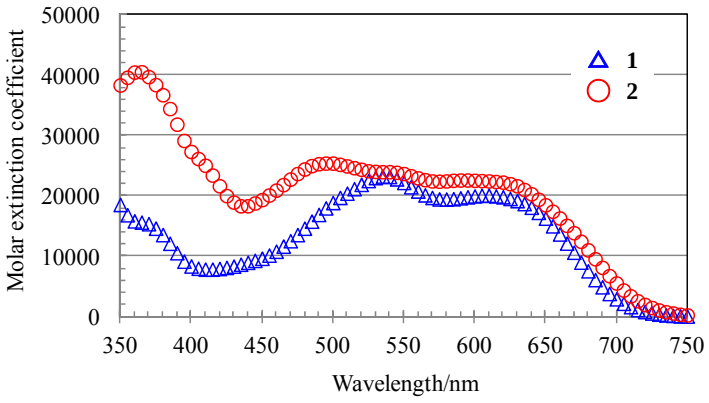

Figure 2 Optical absorption spectra of **1** and **2** in N-methylpyrrolidone.

3.4 Results and Discussion

3.4.1 Optical absorption spectra

The compounds **1** and **2** can slightly dissolve in N-methylpyrrolidone, and their solution of 28.3 μm/L and 19.7 μm/L, respectively, were prepared to evaluate molar extinction coefficients of the compounds. The spectra thus observed were shown in Figure 2. Both compounds exhibit broad and almost structureless bands from 450 to 700 nm covering considerable part of visible light range. The molar extinction coefficients are approximately 20000 or more in the wavelength region of 520 to 650nm and are predominant over those of the red pigments discussed in Chapter 2 or a reference [44].

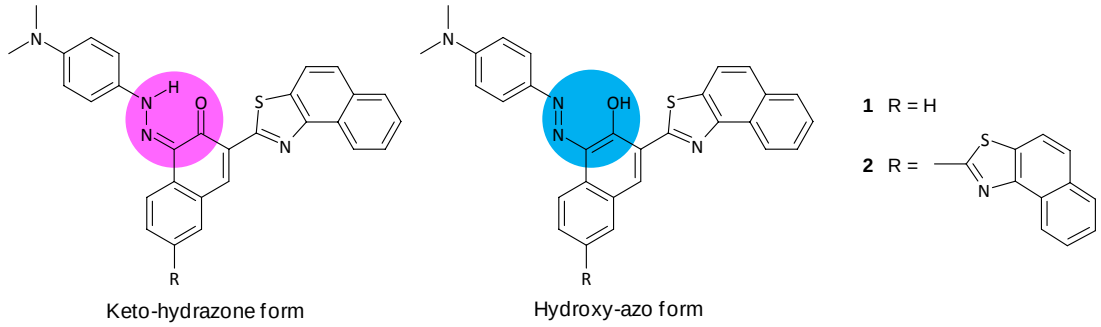

Figure 3 Tautomerism of **1** and **2** between keto-hydrazone (pale red) and hydroxy-azo (pale blue) forms.

3.4.2 Structure determination from powder diffraction data

As shown in Figure 3, there are two possible tautomeric forms for **1** and **2** (keto-hydrazone and hydroxy-azo forms), and it is difficult to distinguish the difference from the powder X-ray diffraction data. The IR spectra of **1** and **2** also gave no clear distinction between the tautomeric forms. Therefore, DFT calculations were carried out to estimate the energy difference of both tautomeric forms. The energy differences were calculated to be 3.92 kcal/mol for **1** and 3.93 kcal/mol for **2**, and the keto-hydrazone forms have lower energies than the hydroxy-azo forms in both molecules, where the total electron energies were used for the calculations converting from Hartree atomic units. The detail investigation using single crystal X-ray diffraction combined with DFT

calculation on the azo-hydrazone tautomerization of similar compounds suggested the hydrazone forms were generally favorable than azo forms [45]. In addition, the literature reported that the energetical difference more than ca. 1 kcal/mol gave complete ordering of the tautomer. The calculated UV/vis spectra of the hydrazone forms (green dash lines in Figure 3) obtained by time dependent DFT (TD-DFT) calculations gave better agreement with those in the solution (red lines in Figure 3) than azo forms (purple dash lines in Figure 3). Here the B3P86 functional with a 6-31G* basis set were used for the TD-DFT calculations because it can give better result than the B3LYP functional [46]. From these considerations, it was concluded that the molecules are in the hydrazone forms in both crystals. The final Rietveld structural refinements were, therefore, carried out with the hydrazone forms. Figure 4 illustrates the experimental and calculated powder X-ray diffraction patterns of **1** and **2** after the refinements, displaying good agreement between those two patterns. The final results are shown in Table 1 [47]. Final R_F^2 are less than 0.1 for **1** and **2**, which ensure reliability of the analyses.

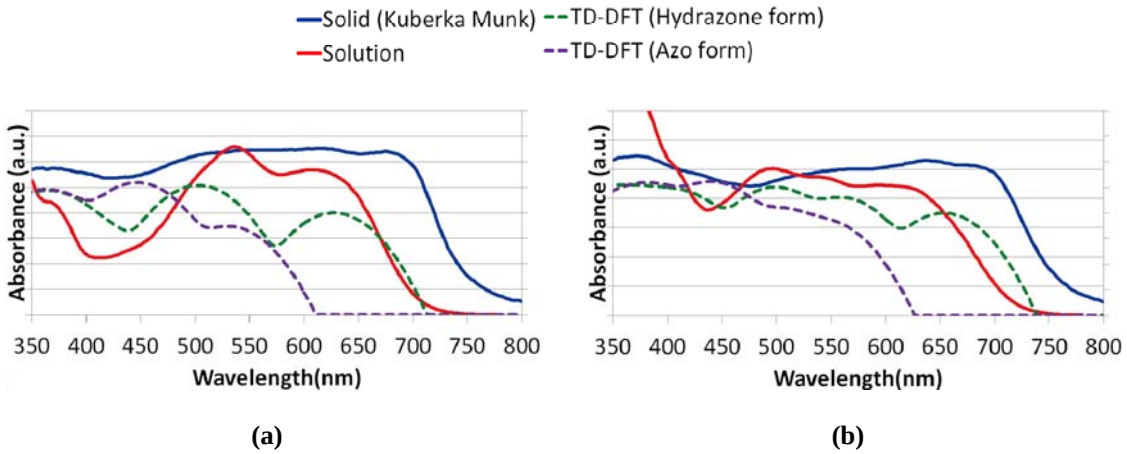

(a) **(b)**

Figure 3 UV/vis spectra of **1** (a) and **2** (b): in solid on Kuberka-Munk conversion (blue), calculated from hydroxy-azo tautomer on TD-DFT (broken green), and calculated from keto-hydrazone tautomer (broken purple). The spectra of **1** and **2** in N-methylpyrrolidone (red) are shown again for easy comparison with those of the solid and the calculations.

(a)

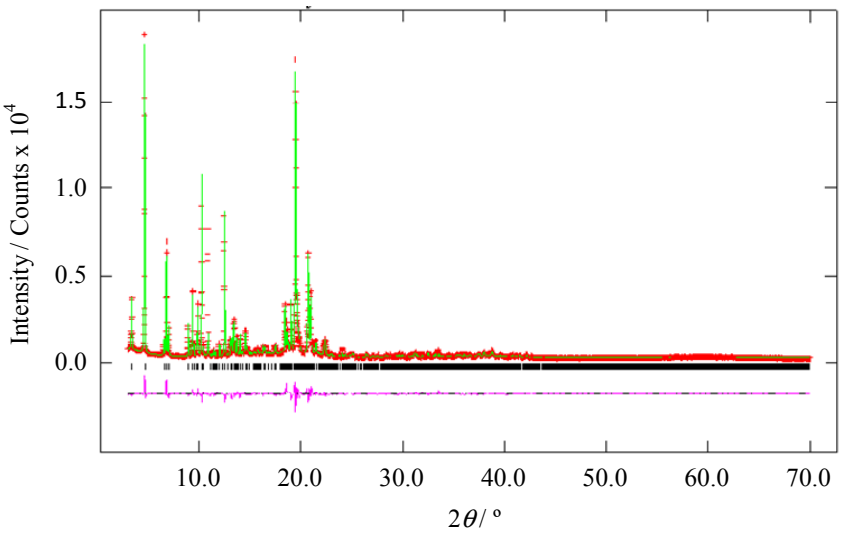

(b)

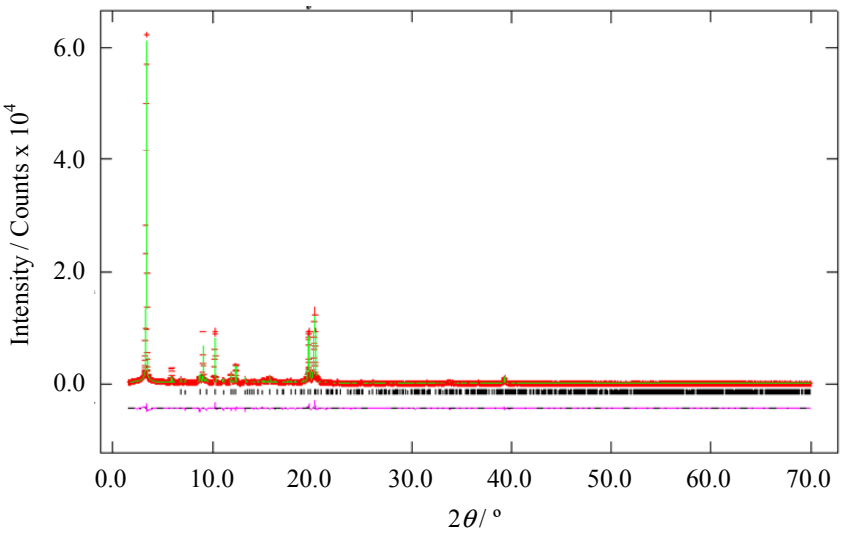

Figure 4 Powder X-ray diffraction patterns obtained from **1** (a) and **2** (b): experimental (red + marks), calculated (green solid line), and difference profile (pink line).

Table 1 Crystallographic data of **1** and **2** [21].

	1	**2**
Formula	$C_{29}H_{22}N_4OS$	$C_{40}H_{27}N_5OS_2$
Formula weight	474.58	657.80
Crystal system	Monoclinic	Hexagonal
Space group	$P2_1/c$	$P6_1$
a / Å	21.9743(4)	23.1191(6)
b / Å	7.46291(7)	23.1191
c / Å	30.6772(7)	10.67304(15)
α / °	90	90
β / °	114.2703(11)	90
γ / °	90	120
V / Å^3	4586.19(17)	4940.39(25)
Temperature / °C	27	27
Z	8	6
Z'	2	1
R_{wp}	0.0528	0.0752
R_F^2	0.0630	0.0725

The crystal structure of **1** (Figure 5) contains two independent molecules in the unit cell (blue and green in the *ac*-plane). Both molecules are almost flat as illustrated in the projection from the *c**-axis, and are alternatively stacked along the *b*-axis giving a herring bone packing motif with approximately 0.3 nm spacing. There is no intermolecular hydrogen bond and only intramolecular hydrogen bond is found at the hydrazone part. Table 2 summarizes the dihedral angles between the least square planes of the naphthol ring and the aromatic ring at 1- or 3-position of the two independent molecules, where the least square planes are calculated using the atomic coordinates obtained by the structure analysis converting the fractional coordinates to the Cartesian ones. The angles are less than 10 degree demonstrating the molecules are highly planar. The planarity of the molecules strongly suggests that the π-conjugation system extends over the molecule.

The molecule in the crystal structure of **2** (Figure 6) is also flat as confirmed by the dihedral angles of less than 4 degree in Table 3 where displays the dihedral angle between the naphthol ring and 6-naphthothiazole. The molecules arrange themselves parallel to the *ab*-plane giving sheet motifs which are stacked along the *c*-axis with approximately 0.3 nm spacing. In this molecule, 6-naphthothiazole is included in the planarity, surely contributing to extension of the π-conjugation system to be much larger than that of **1**. There is a large vacant channel along the *c*-axis at the (0, 0, *z*) in the crystal structure of **2** as emphasized by the red dash circles in Figure 6 (a). The volume of the void is calculated to be 42.2 nm^3/unit cell, and it is possible to incorporate solvents in them. TGA and DTA are simultaneously measured to confirm inclusion of

solvents. The sample of **2** (3.219 mg) were heated at a rate of 5ºC/min, and the TG curve was recorded from 40 ºC to 300 ºC in a dry nitrogen atmosphere with a flux of 20 mL/min. The TGA data of **2** (Figure 7) showed no mass decrease (less than 0.3% weight loss) by heating, which eliminate the possibility containing the solvents in their crystal packing. In addition, the structural analysis gave good quality fitting between the experimental and calculated data (Figure 4b). Therefore, the large channel contains no ordered molecules and it may be filled by air. As well as for **1**, there is no intermolecular hydrogen bond and only intramolecular hydrogen bond is found at the hydrazone part in the crystal structure of **2**.

(a) Projection from *b*-axis

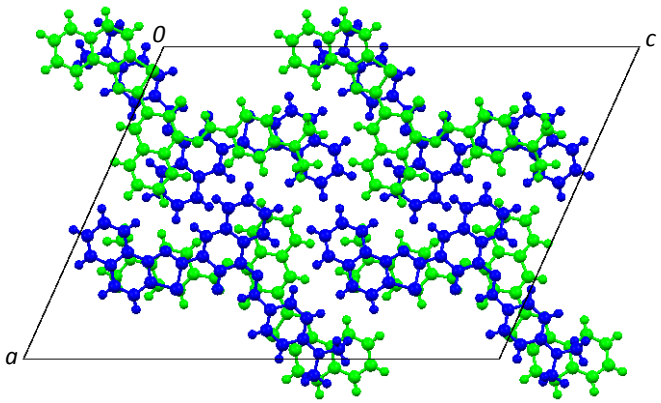

(b) Projection from *c**-axis

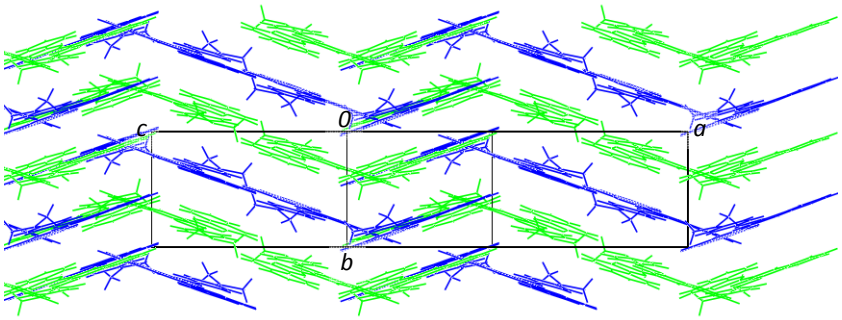

Figure 5 Crystal structure of **1**: (a) Projection onto the (*a*, *c*) plane, and (b) projection from *c**-axis. Two independent molecules are drawn in different colors (blue and green).

(a) Projection from *c*-axis

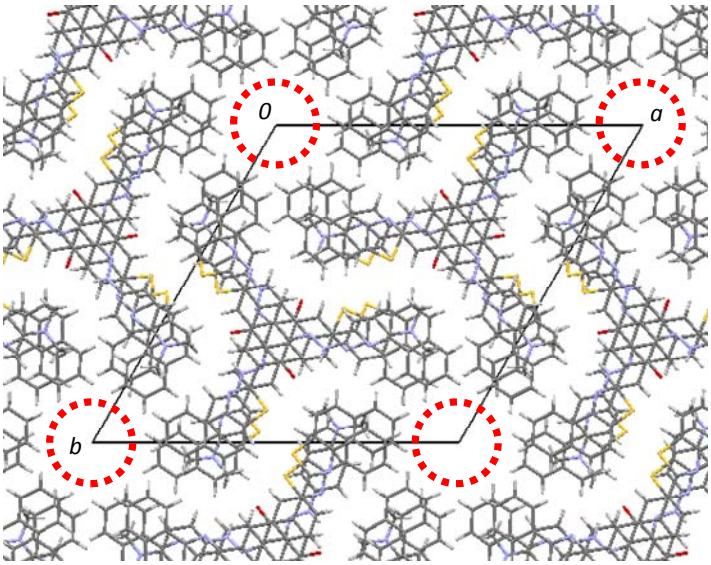

(b) Projection from *b*-axis

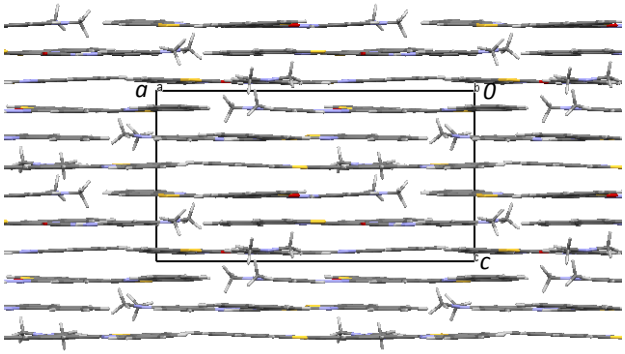

Figure 6 Crystal structure of **2**: (a) Projection onto the (*a*, *b*) plane, and (b) projection onto the (*a*, *c*) lane. Circles of red dash line in (a) represent vacant channels.

Table 2 Dihedral angles between the least square planes of the naphthalene ring and the aromatic ring of **1** and **2**. Molecule I and II of **1** correspond to the independent molecules depicted in green and blue in Figure 5, respectively. The least square planes were calculated by using the atomic coordinates obtained by the crystal structure analyses converting their fractional coordinates to the Cartesian ones.

Position of an aromatic ring (on a naphthalene ring)	Dihedral angle vs. naphthalene (degree)		
	1		**2**
	Molecule I	Molecule II	Unique
1	9.1	3.8	3.6
3	2.7	1.0	3.3
6	–	–	3.3

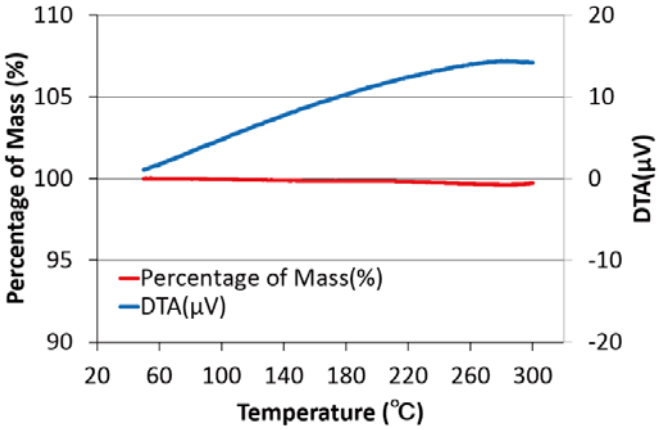

Figure 7 TGA/DTA plot of **2**.

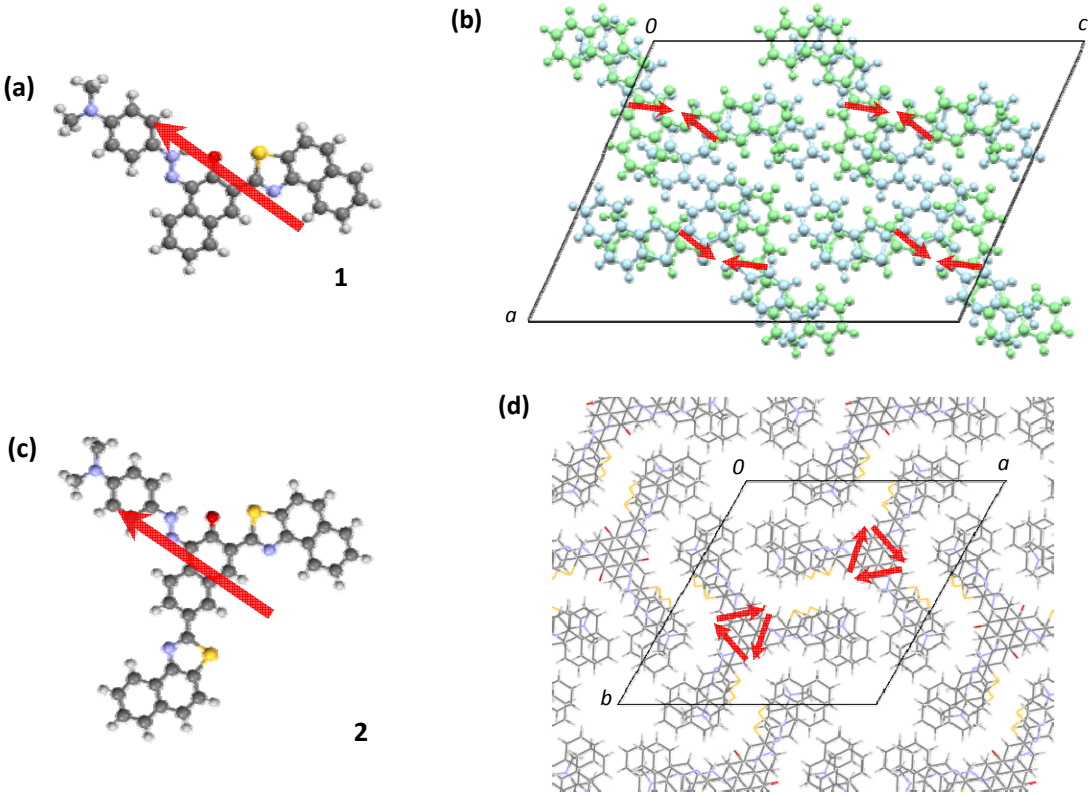

Figure 8 Transition dipole moments of **1** (a) and **2** (c) and their arrangements **1** (b) and **2** (d) in each unit cell. The moments are depicted by the red arrows. In (b), the two crystallographically inequivalent dipoles of **1** align in an oblique fashion. In (d), the three crystallographically equivalent dipoles of **2** helically align around the three-fold screw axes.

UV/vis spectra of both **1** and **2** were measured also in the solid-state (Kuberka Munk conversion of the diffuse reflectance spectra). The absorption bands in the solid-state (blue lines in Figure 3) are shifted to longer wavelength, i.e., red shift, compared to the spectra in the solution (red lines in Figure 3). The red shift of the absorption by crystallization may attribute to the molecular arrangement of the transition dipoles in the crystal structures. It is known that the compound which has high absorption coefficient shows the absorption shift by excitonic interaction [48]. The positions and orientation of two molecules are important for the absorption shift. In the present case, the transition dipoles of **1** and **2** calculated by TD-DFT have oblique arrangements (Figure 8). Such condition is known to lead a Davydov splitting and it would cause broadening of the optical absorption bands in both **1** and **2**, being favorable for substantiating black color.

3.5 Conclusion

In this chapter, two black azo pigments, i.e., 1-(4-dimethyl-amino-phenylazo)-3-naphtho[1,2-d]thiazol-2-yl-naphthalen-2-ol and 1-(4-dimethyl-amino-phenylazo)-3,6-bis-naphtho[1,2-d]thiazol-2-yl-naphthalen-2-ol, were synthesized starting from 3-hydroxy-2-carboxylic acid and 3-hydroxy-2,7-naphthalene dicarboxylic acid, respectively. The pigments exhibit a broad optical absorption band over the visible wavelength region in the solution and solid states. The crystal structures of these pigments were revealed from powder X-ray diffraction data combined with the (TD-)DFT calculations. The DFT calculations suggested the molecules are in hydrazone forms in both crystal structures. Therefore these pigments are actually not azo-type pigments. The both structures consist of the highly planar molecules having largely extended π-conjugation systems which can cause red shift of the optical absorption and a wide variety of electron transitions. The oblique arrangements of the transition dipoles in both crystal structures suggested that the Davydov splitting may occur by the excitonic interactions which cause band broadening of the optical absorption in the crystalline state leading the characteristic black color in the solid state.

Chapter 4

Time-resolved Study of Intramolecular Charge Transfer Fluorescence in 1,2,3,4-Tetra -chloro-11H-isoindolo-[2,1-a]-benzimidazol-11-one

4.1 Abstract

Fluorescent properties of 1,2,3,4-tetrachloro-11H-isoindolo-[2,1-a]-benzimidazol -11-one (TCIB) in various organic solutions are described. Detailed investigation of the fluorescence from the solutions revealed that the fluorescent emission was ascribable to the electronic transition from the lowest singlet excited state of an isolated molecule to its ground state, though the fluorescence spectrum was broad and structureless and the Stokes' shift was about 1 eV. The absorption peak of TCIB was relatively insensitive to change in solvent polarity, whereas its fluorescence peak shifted to the red with an increase in the polarity. This finding suggests that the dipole moment of the molecule in the ground state is almost zero, and that the excited state has a non-zero dipole moment, which coincides with the predicted semi-empirical molecular orbital calculation. Fluorescence quantum efficiency decreased with increase of solvent polarity. The efficiency was reduced by a factor of 39 in going from n-hexane solution to acetonitrile solution. The radiative rate constant also decreased with increase of solvent polarity. However, its reduction was very moderate; the reduction factor was only 2.5 for acetonitrile solution as compared with n-hexane solution. This finding indicates that the emitting state of the title compound is influenced by a solvent-dependent non-radiative mechanism, for which solvent-sensitive intersystem-crossing deactivation is tentatively proposed.

4.2 Introduction

Electron donor-acceptor interaction has been recognized as playing essential roles in the development of optical and electrical properties of organic materials. This type of interaction is also involved in the well-known dual fluorescence of p-(N, N-dimethyl-amino)-benzonitrile, first observed by Lippert [49]. It is generally considered that, upon the electronic excitation, the electron donor–acceptor molecular system changes its conformation so that the donor-acceptor moieties are perpendicular to each other, which leads to a large electronic charge separation between them, and, consequently, to a large dipole moment [50]. This causes solvent-polarity dependence of the fluorescence

emitted by the donor-acceptor interacting system. After the first report on the unusual fluorescence of p-(N,N-dimethylamino)-benzonitrile by Lippert, various compounds, including aminocoumarins [51], biphenyls [52], N-aryl carbazoles [53], and so on, have been investigated from this perspective. In these compounds, solvation of the charge transfer (CT) dipole moment is accompanied more or less by the change in molecular conformation, as is the case for p-(N,N-dimethylamino)-benzonitrile.

In this chapter, the photophysical properties of the intramolecular CT emission of 1,2,3,4-tetrachloro-11H-isoindolo-[2,1-a]-benzimidazol-11-one (TCIB), which was first synthesized by Bistrzycki and Lecco [54], are described in detail. TCIB is a rigid and planar molecule, whose molecular structure is shown at the top of Figure 1, and, consequently, provides a physicochemically interesting opportunity to separate the effects of reorganization and solvation of the CT dipole moment on the CT emission. From this perspective, Wiessner and his co-workers investigated the behavior of rigidly linked pyrene/N-methylindolino derivative and related compounds [55].

TCIB is an attractive compound from a technological as well as a scientific viewpoint. Jaffe discovered [56], 70 years after the first synthesis, that this compound was solid-state fluorescent, and had outstanding photostability for practical application. There are countless numbers of fluorescent organic molecules. However, most of them lack photostability in their isolated molecular states, or, lose their fluorescent properties in return for gaining photostability when they aggregate, because the intermolecular interactions, which bind molecules together, usually enhance non-radiative processes. Only a few molecules, such as derivatives of perylene [57], are both fluorescent and photostable. Thus, TCIB and its derivatives have potential to provide a novel group of molecules that are fluorescent and photostable and also feasible for technological applications.

However, since the first synthesis of TCIB [54], no systematic work on basic physical properties of this compound and its derivatives has been carried out in comparison with the number of reports on perylene derivatives, for example, which are typical aromatic compounds, whose photophysical characteristics have been extensively investigated [58,59]. Crystal structure analysis for TCIB had been conducted in order to gain insight into intermolecular interactions [60]. However, little is known about the photophysical properties of TCIB. The purpose of this chapter is to report the results of a time-resolved measurement of the intramolecular CT type emission for various solutions of this compound.

4.3 Experimental

This compound, synthesized as described elsewhere [56], was dissolved in n-hexane, toluene, diethyl ether, pyridine, acetonitrile, and dimethyl sulfoxide (DMSO), respectively. All of the solvents used in this study were spectrographic grade. No indication of impurity luminescence was observed for the solutions prepared. As-prepared solutions and solutions that had been bubbled with dry nitrogen for 30 min were compared in a spectroscopic way, and no difference was found between them with respect to fluorescence quantum efficiency and fluorescence lifetime.

UV-VIS absorption spectra were measured using a HITACHI U-3300 spectrophotometer. Steady-state fluorescence and fluorescence excitation spectra were recorded using a HITACHI F-4500 fluorescence spectrophotometer. Perylene dissolved in ethyl alcohol was used as the standard of fluorescence quantum efficiency. Its yield is 0.87 when excited at 367 nm. Fluorescence decay time was measured with an in-house time-resolved system using a frequency-tripled Q-switched Nd:YAG laser as excitation. The fluorescent decay curves were analyzed using the conventional deconvolution technique. The decay time was also measured in a frequency domain by phase resolved spectrometry [61] with a Jobin–Yvon–Spex Fluorolog-3 spectrometer equipped with a Tau-3 fluorescence lifetime measurement unit. The decay times measured in the time and the frequency domains gave consistent results.

4.4 Results and discussion

4.4.1 Fluorescence species

The absorption (solid circles with lines) and the fluorescence spectrum (open circles) of toluene solutions are shown in Figure 1. The absorption peak was observed at 372 nm, and the fluorescence peak at 533 nm; the Stokes' shift was abnormally large (about 1 eV), and the fluorescence band was broad and structureless. Its full-width at half-maximum was about 0.5 eV. These are typical characteristics observed for excimer emissions [62,63]. In order to clear up the fluorescence species, the properties of toluene solutions were investigated in detail over a wide range of solute concentrations. Their fluorescent spectra are shown in Figure 2, where they have been normalized for easy comparison. The fluorescence spectra observed for the solutions were same in the solute concentration range from 5.80×10^{-6} up to 3.82×10^{-3} mol/dm^3, which indicates that the emitting state is identical in this concentration range. The solute concentration

dependence of the fluorescence intensity was also investigated, and the results are shown in Figure 3. The thick solid line indicates the linear relation between the intensity and the concentration. The experimental results (open circles) agree well with the line, indicating that the molecules in the solutions are isolated from each other, and in the monomeric state in the solutions. Consequently, it can be concluded that the fluorescence is due to the electronic transition from the lowest singlet excited state of an isolated molecule to its ground state, and not due to dimeric species.

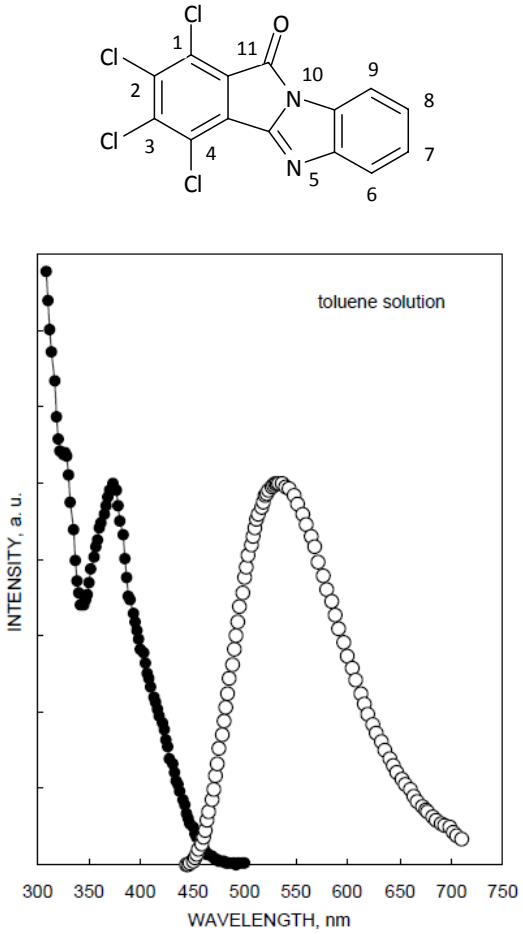

Figure 1 Molecular structure of TCIB is shown at the top of the figure with the atomic numbering. Absorption and fluorescence spectra obtained for toluene solution of TCIB. Solid circles with a line and open circles represent absorption and fluorescence spectra, respectively.

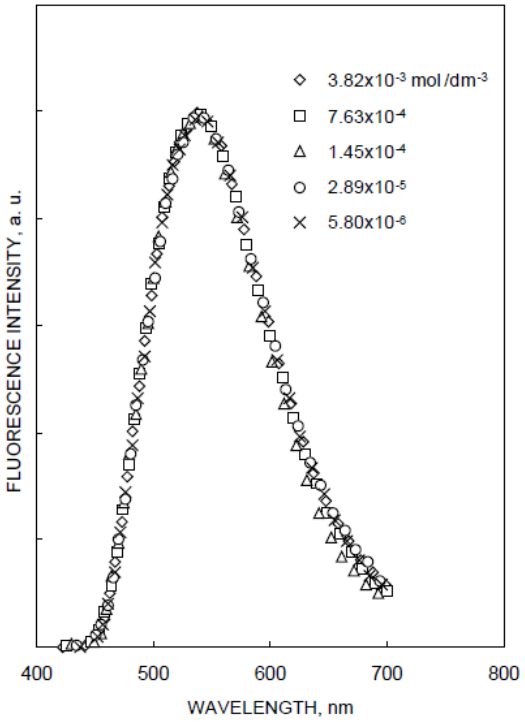

Figure 2 Normalized fluorescence spectra of toluene solution with solute concentration ranging from 5.80×10^{-6} up to 3.82×10^{-3}mol/dm^3.

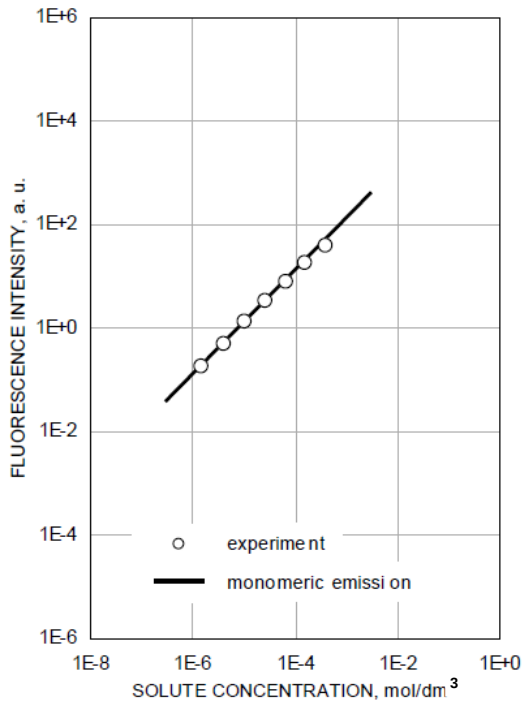

Figure 3 The fluorescence intensity as a function of the solute concentration. The open circles represent experimental results. The thick line represents the linear relation between the intensity and the concentration.

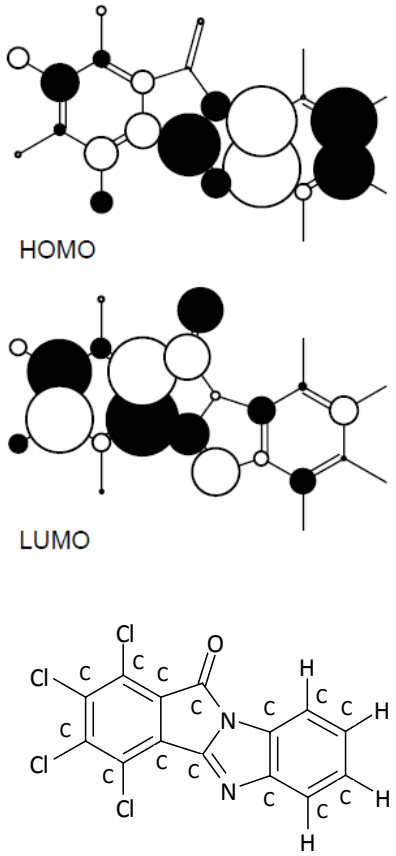

Figure 4 Distribution of the HOMO and the LUMO over a TCIB molecule. Black and white circles represent the difference in the signs of the coefficients when the MOs are represented as linear combinations of atomic orbitals.

4.4.2 Stokes' shift

A feature of fluorescence characteristics of TCIB is a large Stokes' shift. Any of several mechanisms, one of which is change of molecular conformation, can lead to a large Stokes' shift. In order to see the relation between the conformational change and the Stokes' shift of the present compound, semi-empirical molecular orbital (MO) calculation with the AM1 method was carried out.* The optimization was carried out for the molecular conformations of the ground state in a non-polar and a polar matrix, and that of the lowest singlet excited state in a non-polar matrix. One-electron excitation (from the highest occupied molecular orbital [HOMO] to the lowest unoccupied molecular orbital [LUMO]) was taken into consideration for the calculation of the

* WinMOPAC Ver.3, supplied by Fujitsu Limited.

excited state conformation. The calculation revealed that the bond lengths around the nitrogen atom in the isoindole part increased or decreased by a few percent upon the electronic excitation. It also revealed that, for the atoms that have three bonds, the sum of the bonding angles was nearly equal to 360, indicating that the conformation is planar. Consequently, it is concluded that TCIB continues to be planar, in spite of the change in the bond lengths, along with typical changes in the electronic configuration or external environment, and the large Stokes' shift of TCIB does not appear to result from the molecular conformational change such as twisting or bending.

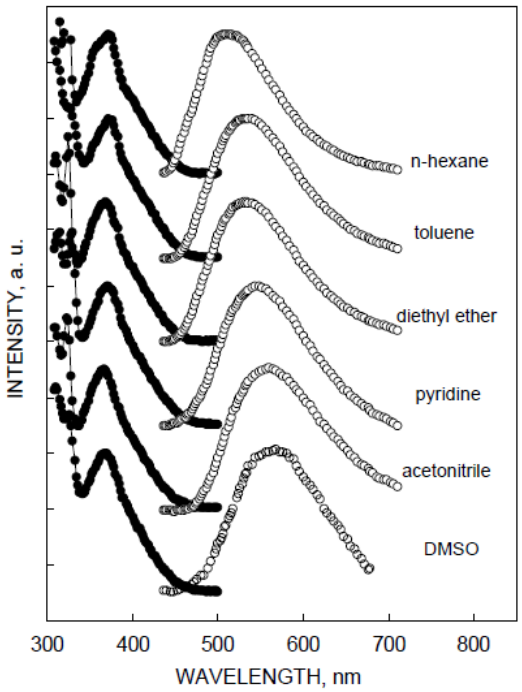

Figure 5 Absorption and fluorescence spectra obtained for various solutions of TCIB. Solid circles with lines and open circles represent absorption and fluorescence spectra, respectively.

Semi-empirical AM1 calculation was also conducted on the HOMO and the LUMO. The results are schematically shown in Figure 4. The radii of the circles on the constituent atoms represent the coefficients by which the atomic orbitals are multiplied to expand the HOMO or the LUMO of TCIB. The open and solid circles represent the signs of the coefficients. It was found that the HOMO is mainly constructed of the

atomic orbitals in the benzimidazole part of the molecule, whereas the LUMO is mainly constructed of the atomic orbitals in the isoindole part of the molecule. These findings indicate that, following the electronic excitation from the HOMO to the LUMO, the electronic redistribution occurs and the dipole moment is induced.

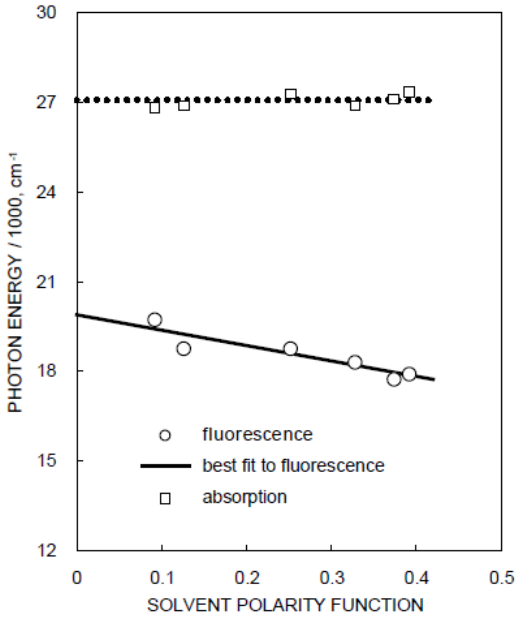

Figure 6 Absorption (open squares) and fluorescence energy (open circles) as functions of the solvent polarity function, which depends upon the static dielectric constant, ε, and the refractive index, n, of the solvent. The absorption peak wavelength is considered insensitive to solvent polarity function. The solid line is the best fit to the experimental results of the fluorescence energies, and its equation is give in the text as Eq. (1).

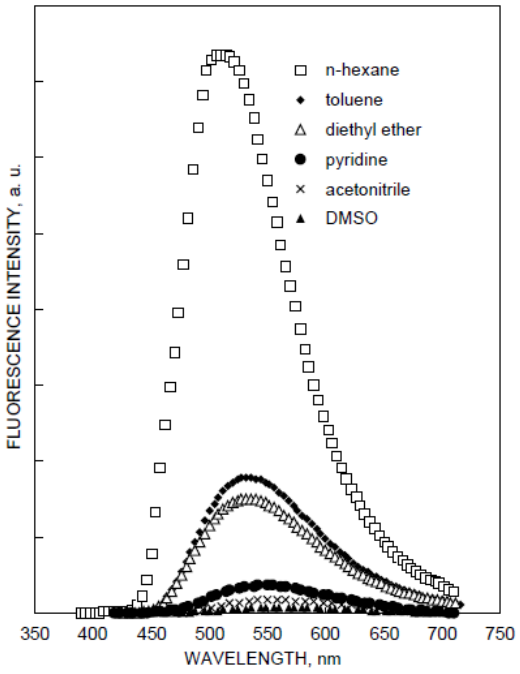

Figure 7 Fluorescence spectra obtained for solutions of n-hexane, toluene, diethyl ether, pyridine, acetonitrile, and DMSO.

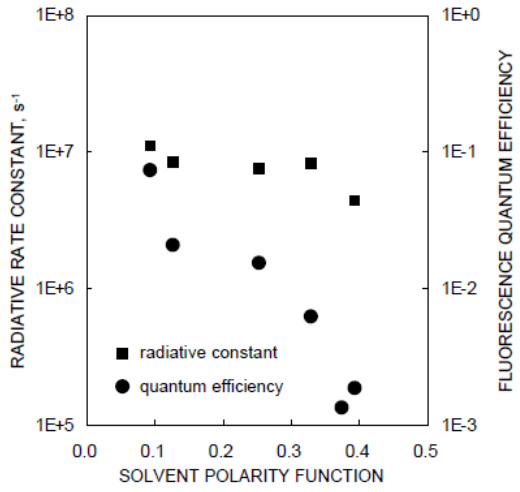

Figure 8 The radiative rate constant (solid squares) and fluorescence quantum efficiency (solid circles) as functions of the solvent polarity function.

Table 1 Absorption wavelength, fluorescence wavelength, fluorescence quantum efficiency, fluorescence lifetime and rate constants of radiative and non-radiative processes of TCIB in various organic solvents.

Solvent	λ_{abs} (nm)	λ_{emis} (nm)	η	τ(s)	k_F (s^{-1})	k_{NR} (s^{-1})
n-Hexane	373	507.4	0.0747	6.70×10^{-9}	1.11×10^{7}	0.14×10^{9}
Toluene	372	532.8	0.0211	2.48×10^{-9}	0.85×10^{7}	0.39×10^{9}
Diethyl ether	367	533.2	0.0153	2.03×10^{-9}	0.75×10^{7}	0.49×10^{9}
Pyridine	372	546.2	0.0063	7.58×10^{-10}	0.83×10^{7}	1.31×10^{9}
Acetonitrile	366	558.2	0.0019	4.31×10^{-10}	0.44×10^{7}	2.32×10^{9}
DMSO	369	563.2	0.0014			

In order to acquire information on the dipole moment, the effects of the solvent polarity on the absorption and the fluorescence energy were analyzed. The absorption spectra of n-hexane, toluene, diethyl ether, pyridine, acetonitrile, and DMSO solutions of TCIB are shown in Figure 5 (solid circles with lines). The absorption peak was observed in the 373-366nm wavelength region, and was relatively insensitive to solvent polarity; this insensitivity is also indicated by open squares as a function of the solvent polarity function in Figure 6. The results are summarized in Table 1. The fluorescence spectra of n-hexane, toluene, diethyl ether, pyridine, acetonitrile, and DMSO solutions are shown in Figure 5 (open circles). The fluorescence peak shifted to the red with increase of solvent polarity, in contrast to the absorption peak. The peak was at 507.4nm for the n-hexane solution, and it shifted up to 563.2nm for the DMSO solution. This finding suggests that the emitting state has an intramolecular charge transfer (ICT) characteristic. The results are shown as a function of the solvent polarity function in Figure 6 (open circles). The solid line is the best fit to the results obtained with the least-square fitting procedure, which is expressed as

$$\nu_{\mathrm{EMIS}} = -5.12 \times 10^{3} \times f(\varepsilon, n) + 19.87 \times 10^{3} \quad (1)$$

where $f(\varepsilon, n)$ is the solvent polarity function, which is expressed as

$$f(\varepsilon, n) = \frac{\varepsilon - 1}{2\varepsilon + 1} - \frac{1}{2}\frac{n^2 - 1}{2n^2 + 1} \quad (2)$$

using the static dielectric constant, ε, and the refractive index, n, of a solvent. The fluorescence energies in the various solvents are summarized in Table 1. The solvent polarity also had a drastic influence on the fluorescence intensity. The increase in polarity caused a reduction of the fluorescence quantum efficiency η. The results are given in Figure 7. The efficiency was 0.0747 for the n-hexane solution, and decreased to

0.0014 for the DMSO solution. The efficiency η is also shown as a function of the solvent polarity function in Figure 8.

The effects of the solvent polarity on the absorption and the fluorescence energy were investigated in order to acquire information on the dipole moment change before and after the excitation. Based on the Onsagar concept of a reaction field created in the solution by a solute dipole moment located at the center of spherical cavity with radius a_0, the absorption energy can be expressed as [64]

$$h\nu_{\mathrm{ABS}} = h\nu_{\mathrm{ABS}}^{\mathrm{VAC}} + \frac{2\mu_{\mathrm{g}}(\mu_{\mathrm{g}} - \mu'_{\mathrm{e}})}{a_0^3}\left[\frac{\varepsilon - 1}{2\varepsilon + 1} - \frac{1}{2}\frac{n^2 - 1}{2n^2 + 1}\right] + \frac{\mu'_{\mathrm{e}}(\mu_{\mathrm{g}} - \mu'_{\mathrm{e}})}{a_0^3}\left[\frac{n^2 - 1}{2n^2 + 1}\right] \quad (3)$$

where $h\nu_{\mathrm{ABS}}$ and $h\nu_{\mathrm{ABS}}^{VAC}$ stand for the absorption energy in the solvent and the vacuum, respectively, and μ_{g} and μ'_{e} for the dipole moments of the solute in the ground and the Franck–Condon excited states, respectively. If the Franck–Condon excited state is the same as the equilibrium excited state in nature, then we can approximate $\mu'_{\mathrm{e}} = \mu_{\mathrm{e}}$, where μ_{e} is the dipole moment of the solute in the equilibrated excited state. The refractive index does not vary greatly from solvent to solvent. Therefore, the third term in Eq. (3), relative to the second term, can be treated as constant. As shown in Figure 6, the absorption energy was independent of the solvent polarity function. This indicates that $\mu_{\mathrm{g}} \approx 0$.

A similar equation is obtained for the fluorescence energy, which can be expressed as [64]

$$h\nu_{\mathrm{FLU}} = h\nu_{\mathrm{FLU}}^{\mathrm{VAC}} + \frac{2\mu_{\mathrm{e}}(\mu'_{\mathrm{g}} - \mu_{\mathrm{e}})}{a_0^3}\left[\frac{\varepsilon - 1}{2\varepsilon + 1} - \frac{1}{2}\frac{n^2 - 1}{2n^2 + 1}\right] + \frac{\mu'_{\mathrm{g}}(\mu'_{\mathrm{g}} - \mu_{\mathrm{e}})}{a_0^3}\left[\frac{n^2 - 1}{2n^2 + 1}\right] \quad (4)$$

where $h\nu_{\mathrm{FLU}}$ and $h\nu_{\mathrm{FLU}}^{\mathrm{VAC}}$ stand for the fluorescence energy in the solvent and the vacuum, respectively, and μ'_{g} and μ_{e} for the dipole moments of the solute in the Franck–Condon ground and the equilibrium excited states, respectively. If the Franck–Condon ground state is the same as the equilibrium ground state in nature, then we can approximate $\mu'_{\mathrm{g}} = \mu_{\mathrm{g}}$. As shown in Figure 6, the fluorescence energy decreased with increase in the solvent polarity function, which indicates that, according to Eq. (4), $\mu_{\mathrm{e}} \neq 0$ and $\mu_{\mathrm{g}} - \mu_{\mathrm{e}} \neq 0$.

The interpretation that consistently explains the solvent dependence of the

absorption and the fluorescence energy is that $\mu_g \approx 0$ and $\mu_g - \mu_e \neq 0$. In order to confirm this interpretation, the dipole moments were estimated with the AM1 MO calculation for the ground and the lowest singlet excited S_1 state. The moments were evaluated to be 0.4 and 14.2 Debye for the ground and the excited state, respectively. These calculated results are consistent with the above interpretation. Further, assuming the third term in Eq. (4) is solvent independent and $\mu_g \approx 0$, the value of μ_e was determined from the experimental results on solvent dependence of the fluorescence energy. The value thus determined was 15.2 Debye, which is close to the calculated value (14.2 Debye), clearly showing that the interpretation that $\mu_g \approx 0$ and $\mu_g - \mu_e \neq 0$ coincides with the experimental and the calculated results.

Combining these results with the above-mentioned MO calculations of the HOMO and the LUMO (Figure 4), the following can be surmised: TCIB has a negligible dipole moment in the ground state. However, it has a large dipole moment (14.2 Debye) in the lowest singlet excited state. For the atomic orbitals constructing the HOMO and the LUMO distributed in the benzimidazole and the isoindole parts of the molecule, respectively, the ICT occurs following the electronic excitation. Also, the solvation takes place for the Franck–Condon excited state to be equilibrated. These events may explain why a large Stokes' shift is observed in TCIB, though no conformational change occurs.

4.4.3 Solvent-polarity dependent non-radiative mechanism

Fluorescence lifetime was measured for the solutions prepared in this study. The fluorescence decay was well approximated with a single exponential function when the solvent was less polar. In the case of polar solutions, it was necessary to use a double exponential function to reproduce its fluorescent decay. The lifetime τ was 6.70 ns for the n-hexane solution, which decreased with increase of solvent polarity, and 0.43 ns for the acetonitrile solution.

Combining these results with the fluorescent quantum efficiency η shown in Figure 8, the radiative and non-radiative rate constants for the solutions were obtained as $k_F = \eta/\tau$, and $k_{NR} = [1 - \eta]/\tau$, respectively. Photophysical parameters obtained are summarized in Table 1. The radiative rate constants thus determined are shown in Figure 8 as a function of the solvent polarity function. The fluorescent efficiency decreases very rapidly with solvent polarity. The efficiency was reduced by a factor of 39 in going from the n-hexane solution to the acetonitrile solution. On the other hand, the radiative rate constant is rather insensitive to the solvent polarity; it was 1.11×10^7

s^{-1} in the n-hexane solution and 0.44×10^7 s^{-1} in the acetonitrile solution. The reduction factor was only 2.5 for the radiative rate constant. In this respect, its emitting state is different from the ICT state of coumarin 334, for example, for which the fluorescence peak wavelength shifts to the red, and its quantum efficiency is only slightly affected by solvent polarity [51]. Evidently, there is a solvent-dependent non-radiative mechanism accompanying the ICT state of TCIB.

Generally, there are two possible ways in which an ICT state is expressed by a solvent-dependent non-radiative mechanism. One is the case in which the ICT sate wave function, Φ_{EX}, is expressed as a linear combination of a neutral pair, an ionized pair, and a Franck–Condon excited state of an electron-donating and an electron-accepting group, Φ[AD], Φ [A^-D^+], and Φ [FC^*], as originally proposed for exciplexes and excited complexes [65].

$$\Phi_{EX} = C_0\Phi[AD] + C_1\Phi[A^+D^-] + C_2\Phi[FC^*]. \quad (5)$$

The exact character of Φ_{EX} is dependent on the coefficients C_0, C_1, and C_2, which are solvent polarity dependent. In the other case, the ICT state is accompanied by a state characterized by a solvent dependent non-radiative mechanism such as twisted ICT (TICT). The α-dicarbonyl-substituted coumarin is an example of this type [50].

The fluorescence efficiency and the lifetime decrease remarkably with solvent polarity for TCIB, whereas its radiative rate constant is relatively insensitive to solvent polarity, as shown in Figure 8. If the ICT state of the present compound could be expressed as Eq. (5), its radiative rate constant would decrease with solvent polarity, based on the expectation that the contribution of the ionized-pair increased in polar solvent. Therefore, it is considered that the emitting state of TCIB may be expressed as the ICT state, which is accompanied by a second ICT state with a solvent-dependent non-radiative path.

Next, let us consider the origin of the state characterized by a solvent-dependent non-radiative mechanism. In the case of α-dicarbonyl-substituted coumarin [51], it is proposed that the TICT state originates from the rotation related to the bond connecting its two carbonyl groups. The present compound, however, is planar and rigid, and does not change its conformation as described above. Therefore, a second ICT state with different conformation is not available to provide a solvent-sensitive non-radiative path.

In some compounds for which ICT type emission is observed, intersystem crossing from the ICT emitting state to a triplet state is proposed or supposed [66]. The semi-empirical intersystem crossing rate is given by [67]

$$k_{\mathrm{ISC}}(\mathrm{S}^1 \rightarrow \mathrm{T}^i) = 10^{12}\left|\beta_{\mathrm{S}^1\mathrm{T}^i}\right|^2 \exp\left(-0.25E^{0.4}_{\mathrm{S}^1\mathrm{T}^i}\right) \qquad (6)$$

where $\left|\beta_{\mathrm{S}^1\mathrm{T}^i}\right| = \langle\phi_{\mathrm{S}}|\mathrm{H}_{\mathrm{SO}}|\phi_{\mathrm{T}}\rangle$ stands for the matrix element of the spin–orbit coupling of S_1 and T_i, $E_{\mathrm{S}^1\mathrm{T}^i}$ for the energy gap between S_1 and T_i expressed in cm^{-1}. Therefore, the intersystem crossing rate, k_{ISC}, is dependent on the singlet-triplet energy gap. In addition, it is theoretically predicted that the singlet energy is stabilized with respect to the triplet energy as a result of the interaction with the solvent [68]. This means that the energy gap $E_{\mathrm{S}^1\mathrm{T}^i}$ is decreased with the increase in the solvent polarity, which, according to Eq. (6), causes enhancement in the intersystem crossing rate. This may explain why the radiative rate constant was relatively insensitive to, and the fluorescence efficiency decreased drastically with, increase in the solvent polarity function.

4.5 Conclusion

Steady state and time-resolved fluorescence measurement were carried out for various organic solutions of TCIB. Detailed investigation of the solutions revealed that the fluorescence is ascribable to the electronic transition from the lowest singlet excited state of an isolated molecular state to its ground state. The absorption peak, observed in the 373-366nm wavelength region, was relatively insensitive to solvent polarity. The fluorescence peak shifted to the red with increase of solvent polarity. The peak was at 507.4nm for the n-hexane solution, and it shifted up to 563.2nm for DMSO solution. It can be interpreted that $\mu_{\mathrm{g}} \approx 0$ and $\mu_{\mathrm{e}} = 15.2$ Debye, which coincides with the semi-empirical MO calculation.

The fluorescence efficiency was decreased with increase of solvent polarity. The efficiency was 0.0747 for the n-hexane solution, and decreased to 0.0019 for the acetonitrile solution. The radiative rate constant also decreased with increase of solvent polarity. However, the reduction was very moderate. The rate constant was 1.11×10^7 s^{-1} for the n-hexane solution, and decreased by a factor of only 2.5 (0.44×10^7 s^{-1}) for the acetonitrile solution. This indicated that the emitting state of the present compound is influenced by a solvent dependent non-radiative mechanism, for which intersystem crossing is tentatively proposed.

Chapter 5

Thesis Conclusion

Organic pigments are the requisite materials in our life. In particular, azo pigments have been an important subclass of colorants. Various kinds of arylides derived from 3-hydroxy-2-naphthoic acid have provided many kinds of azonaphtharylamide pigments, and alteration of this mono carboxylic acid to 3-hydroxy-2,7-naphthalene dicarboxylic acid enabled exploration into further diversity of azo pigments. The above dicarboxylic acid can provide 7-arylamide, and presence of the 7-arylamide distinguishes the resultant pigments from conventional azonaphtharylamide pigments. The 7-substituent in the two red pigments synthesized in Chapter 2 did not cause bathochromic shift but provided hyperchromic effects in solution compared with the 7-unsubstituted counterparts. Molecular orbital (MO) calculations, including structure optimizations for keto-hydrazone configuration, suggested that the 7-substituent is involved in the electron transitions while the substituent is hardly involved in the π-conjugation systems. The pigments showed better light-fastness than the 7-unsubstituted counterparts probably due to increment of the number of the amide groups. Drastic modification in chemical structures of azo pigments was further advanced in Chapter 3 aiming at materializing black azo pigments, where the structure was modified from arylamide-type to non-arylamide type to extend the π-conjugation systems. The two pigments having naphthothiazole(s) via carbon-carbon linkage were prepared from 3-hydroxy-2-naphthoic acid and 3-hydroxy-2,7-naphthalene dicarboxylic acid. The pigments exhibited characteristic black hue for the category of azo pigments. Crystal structure analyses from powder X-ray patterns combined with DFT calculations revealed that the two pigments have keto-hydrazone configurations and are highly planar promoting extension of the π-conjugation systems. The arrangements of the transition dipoles in the crystal structures were oblique fashion, suggesting that Davydov splitting may occur by the excitonic interactions. The splitting is expected to assist black hue by the red and/or blue absorption band shift(s) in the crystalline state in addition to the extended π-conjugation systems. The results of Chapters 2 and 3 clearly demonstrate that azo pigment can be diversified by drastic modification of the chemical structures to expand horizons of this category.

Fluorescent pigments are important substances besides inorganic and organic pigments. In particular, organic fluorescent materials which fluoresce in the solid state are of great interest. Of various organic solid-state-fluorescent compounds,

1,2,3,4-tetrachloro-11H-isoindolo-[2,1-a]-benzimidazol-11-one (TCIB) is a unique and distinct molecule in its excellent and practical photostability. Fluorescent behavior of this compound in some organic solvents of various polarities was studied using MO calculation, steady state and time-resolved spectroscopy. The fluorescence spectra of the compound were broad and structureless, resembling the characteristics from an excimer state. It was concluded that the emission was ascribable to the deactivation from the LUMO of an isolated molecule to the HOMO, i.e. not an excimer emission, where the LUMO has a non-zero dipole moment formed through intramolecular charge transfer following excitation from the HOMO whose dipole moment is almost zero. The solvent polarities varied largely the fluorescence quantum efficiencies and moderately the radiative rate constants, although the absorption maxima were insensitive to the solvent polarities. These results indicate that the emitting state of the compound is influenced by a solvent-dependent non-radiative deactivation process, for which solvent-sensitive intersystem-crossing can be proposed.

In summary, the author prepared four novel azo pigments in the present study, and revealed their fundamental properties. The results indicate that historically old azo pigment yet has had potential for expansion of its horizons. Regarding the category of organic fluorescent pigments, the author investigated a scientifically interesting organic solid-state-fluorescent compound in detail and revealed its emitting state. The outcome of the present thesis will be useful information for research and development of functional colorants.

References

[1] W. Herbst, K. Hunger, Industrial Organic Pigments, Third edition, Wiley-VCH, Weinheim, 2004.

[2] R.M. Christie, Colour Chemistry, Royal Society of Chemistry, Cambridge, 2001.

[3] P. Gregory, High-Technology Applications of Organic Colorants, Springer Science+Business Media, 1991.

[4] K. Sato, K. Hino, H. Takahashi, J. Mizuguchi, Int. J. Intelligent Systems Technologies and Applications, 3 (2007), 52-62.

[5] J. Mizuguchi, J. Appl. Phys. 66 (1989), 3111-3113.

[6] H. Takahashi, J. Mizuguchi, J. Electrochem. Soc. 152 (2005), H69-H73.

[7] H.M. Smith (ed.), High Performance Pigments, Wiley-VCH, Weinheim, 2002.

[8] C. W. Tan, Appl. Phys. Lett. 48 (1986), 183-185.

[9] J. Otani, H. Yamamoto, N, Dan, A. Iqbal, R. Moretti, Electroluminescent devices comprising diketopyrrolopyrroles, Ciba Specialty Chemicals Holding Inc., European Patent, EP1329493A1, 2003.

[10] H. Langhals, T. Potrawa, H. Noth, Angew. Chem. Int. Ed. Engl. 28 (1989), 478-480.

[11] T. Tanaka, Color liquid crystal display device, T. Tanaka and Dai Nippon Printing Co., Ltd., US Patent US2003/0053013, 2003.

[12] S. Matsumoto, T. Yanagisawa, Organic white pigments, Hakko Chemical Co., Ltd., US Patent 5514213, 1996.

[13] H. Sakiyama, K. Bessho, Hollow particle for white ink for inkjet, method for producing the same and white ink for inkjet, JSR Corporation, Japanese Patent JP2009-035672, 2009.

[14] J. Mizuguchi, N. Shimo, J. Imaging Sci. Technol., 50 (2006), 115-121.

[15] E.E. Jaffe, Fluorescent yellow 1,2,3,4-tetrachloro-11H-isoindolo- not 2,1-a -benzimidazol-11-one pigment, CIBA-GEIGY AG, European Patent EP0456609A1, 1991.

[16] R. Ueno, J. Otani, T. Yamashita, T. Hisano, Red ink composition for color filter, Ueno Institute for Chemical Science, European Patent EP1693426A1, 2006.

[17] R. Ueno, J. Otani, T. Yamashita, T. Hisano, Monoazo compound and method for producing same, Ueno Institute for Chemical Science, European Patent EP1650267A1, 2006.

[18] S.R. Sandler, W. Karo, Sourcebook of advanced organic laboratory preparations, First edition, Academic Press, Inc, London, 1992.

[19] R. M. Christie, C. H. Chang, H. Y. Huang, M. Vincent, Surf. Coat. Int., Part B, Coat Transact. 89 (2006), 77–85.
[20] R. Ueno, M. Kitayama, K. Minami, H. Wakamori, Azo compounds and process for producing the same, Ueno Institute for Chemical Science, European Patent EP1048694A1, 2000.
[21] C.H. Chang, R.M. Christie, G. M.Rosair, Dyes and Pigments 82 (2009), 147-155.
[22] A. Whitaker, J. Soc. Dyes Color 69 (1978), 431-435.
[23] P. Gilli, V. Bertolasi, L. Pretto, L. Antonov, G. Gili, J. Am. Chem. Soc. 127 (2005), 4943-4953.
[24] A. Whitacker, Z. Kristallogr. 146 (1977), 173-184.
[25] D. Kobelt, E. F. Paulus, W. Kunstman, Z. Kristallogr. 139 (1974), 15-32.
[26] D. Kobelt, E. F. Paulus, W. Kunstman, Acta Cryst. B28 (1972), 1319-1324.
[27] W. M. F. Fabian, S. Schuppler, O. S. Wolfbeis, J. Chem. Soc., Perkin Trans. 2 (1996), 853-856.
[28] M. Adachi, Y. Murata, S. Nakamura, J. Org. Chem. 58 (1993), 5238-5244.
[29] A. Iqbal, M. Jost, R. Kirschmayr, J. Pfenniger J, A. Rochat, O. Wallquist, Bull. Soc. Chim. Belg. 97 (1988), 615-644.
[30] J. Mizuguchi, T. Senju, J. Phys. Chem. B 11 (2006), 19154-19161.
[31] J. Mizuguchi and N. Shimo, J. Imaging Sci. Thechnol. 50 (2006), 115-121.
[32] R.M. Christie, Colour Chemistry, Royal Society of Chemistry, Cambridge, 2001, p. 52.
[33] A. D. Towns, Dyes and Pigments 42 (1999), 3-28.
[34] M. Speckbacher, J. Chassot, H-J. Braun, Dark colored azo dyes, The Procter & Gamble Company, International Patent Publication WO2008/050295, 2008.
[35] K. D. M. Harris and M. Tremayne, Chem. Mater. 8 (1996), 2554-2570.
[36] K. D. M. Harris, M. Tremayne and B. M. Kariuki, Angew. Chem. Int. Ed. 40 (2001), 1626-1651.
[37] H. Tsue, M. Horiguchi, R. Tamura, K. Fujii and H. Uekusa, J. Synth. Org. Chem. Japan 65 (2007), 1203-1212.
[38] E. Mohasci and J. P. O'Brien, Naphtho[1,2-b][1,4]thiazepin-4(5H)-ones and use thereof in treatment of ischemia and blood pressure lowering, Hoffmann-La Roche Inc. United States Patent 480850(A), 1989.
[39] M. A. Neumann, J. Appl. Cryst. 36 (2003), 356–365.
[40] A.Boultif and D. Louër, J. Appl. Crystallogr. 37 (2004), 724-731.
[41] W. I. F. David, K. Shankland, J. Cole, S. Maginn, W. D. H. Motherwell and R. Taylor, DASH User Manual. Cambridge Crystallographic Data Centre,

Cambridge, UK 2001.
[42] H. M. Rietveld, J. Appl. Cryst. 2 (1969), 65-71.
[43] A. C. Larson, R. B. Von Dreele, GSAS; Los Alamos Laboratory Report No. LA-UR-86-748; Los Alamos National Laboratory: Los Alamos, NM, 1987.
[44] J. Otani, T. Kikuchi, S. Higashida, T. Harada and M. Matsumura, J. Mol. Str. 1084 (2015), 28-35.
[45] P. Gilli, V. Bertolasi, L. Pretto, L. Antonov and G. Gilli, J. Am. Chem. Soc. 127 (2005), 4943-4953.
[46] L. B. Wiberg, R. E. Stratmann and M. J. Frisch, Chem. Phys. Lett. 297 (1998), 60-64.
[47] Crystallographic data reported in this chaper have been deposited with Cambridge Crystallographic Data Centre as supplementary publication no. CCDC 1043710 and 1043711. Copies of the data can be obtained free of charge via www.ccdc.cam.ac.uk/conts/retrieving. html (or from the Cambridge Crystallographic Data Centre, 12, Union Road, Cambridge, CB2 1EZ, UK; fax: +44 1223 336033; or deposit@ccdc.cam.ac.uk).
[48] J. Mizuguchi, J. Soc. Photo. Sci. Tech. Japan, 70 (2007), 268-277.
[49] E. Lippert, W. L.uder, H. Boss, in: A. Mangini (Ed.), Advances in Molecular Spectroscopy, Pergamon Press, Oxford, 1962, p. 443.
[50] K. Rotkiewicz, K.H. Grellmann, Z.R. Grabowski, Chem. Phys. Lett. 19 (1973), 315-318.
[51] J.A. Van Gompel, G.B. Schuster, J. Phys. Chem. 92 (1989), 1292-1295.
[52] N. Tamai, I. Yamazaki, H. Masuhara, N. Mataga, Chem. Phys. Lett. 104 (1984), 485-488.
[53] W. Rettig, M. Zander, Chem. Phys. Lett. 87 (1982), 229-234.
[54] A. Bistrzycki, A. Lecco, Helv. Chim. Acta. 4 (1921), 425.
[55] A. Wiessner, W. K.uhnle, T. Fiebeg, H. Staerk, J. Phys. Chem. A 101 (1997), 350-359.
[56] E.E. Jaffe, Fluorescent yellow 1,2,3,4-tetrachloro-11H-isoindolo- not 2,1-a -benzimidazol-11-one pigment, European Patent EP0456609A1,1991.
[57] H. Quante, Y. Geerts, K. Müllen, Chem. Mater. 9 (1997), 495-500.
[58] S. Demmig, H. Langhals, Chem. Ber. 121 (1988), 225-230.
[59] N. Nijegorodov, D.P. Winkoun, Spectrochim. Acta Part A 53 (1997), 2013-2022.
[60] J. Otani, N. Hirayama, T. Deno, K. Kodama, to be submitted.
[61] J.R. Lakowicz, Principles of Fluorescence Spectroscopy, Plenum Press, New York, 1983.

[62] J.B. Birks, L.G. Christophorou, Proc. R. Soc. A 274 (1963), 552-564.
[63] J.B. Birks, L.G. Christophorou, Proc. R. Soc. A 277 (1964), 571-582.
[64] N. Mataga, Y. Kaifu, M. Koizumi, Bull. Chem. Soc. Jpn. 29 (1956), 465-470.
[65] I.R. Gould, R.H. Young, L.J. Mueller, A.C. Albrecht, S. Farid, J. Am. Chem. Soc. 116 (1994), 8188-8199.
[66] J. Herbich, A. Kapturkiewicz, Chem. Phys. 158 (1991), 143-153.
[67] N. Nijegododov, V. Ramachandran, D.P. Winkoun, Spectrochim. Acta A 53 (1997), 1813-1824.
[68] C. Gonzalez, A. Restrepo-Cossio, M. M!arquez, K.B. Wiberg, M. Rosa, J. Phys. Chem. A 102 (1998), 2732-2738.

Acknowledgements

The author, myself, must emphasize and acknowledge that completion of this thesis was impossible without the support of many people. The first and foremost, I wish to express my deepest gratitude to Professor Takeshi Kikuchi of Ritsumeikan University for his carefully reviewing my dissertation and cordial encouragement to my research. I greatly appreciate Professor Emeritus Michio Matsumura of Osaka University for his guidance. I would like to thank Professor Hidehiro Uekusa and Dr. Kotaro Fujii of Tokyo Institute of Technology for invaluable collaboration and discussion on crystal structure analyses. I express my appreciation from the bottom of my heart to Professor Suguru Higashida (Osaka Prefecture University College of Technology), Dr. Takashi Harada and Mr. Akira Kimura (both Osaka University) for their selfless help and support on some of the instrumental analyses. I would like to sincerely acknowledge the induction and constant guidance in knowledge of organic pigments by Dr. Abul Iqbal of IQ Consult GmbH, Switzerland, since the initial stage of my career as a researcher. I give thanks to my ex-colleagues at Ueno Fine Chemicals, Co., Ltd, particularly to Messrs. Tetsuya Yamashita, Takaya Hisano and Shigeji Mori. The discussion with them always stimulated and motivated me. Finally, I am deeply grateful to my family, Naomi, Ikuki and Ikuho, especially my wife Naomi, who made my studies possible by her support at home.

Publications

Scientific Papers

1. J. Otani, T. Kikuchi, S. Higashida, T Harada and M. Matsumura, "Synthesis and properties of azonaphtharylamide pigments having arylamide groups at 2- and 7-positions", Journal of Molecular Structure, **1084** (2015), pp. 28-35.

2. J. Otani, M. Matsumura, K. Fujii and H. Uekusa, "Structure determination from powder X-ray diffraction data of black azo (hydrazone) pigments", Chemistry Letters, **44** (2015), pp. 662-664.

3. J. Otani, H. Yamamoto, M. Fukuda and K. Kodama, "Time-resolved study of intramolecular charge transfer fluorescence in 1,2,3,4-tetrachloro-1H-isoindolo-[2, 1-a]-benzimidasol-11-one", Journal of Luminescence, **104** (2003), pp. 273-281.

International conference

- J. Otani, K. Chiba and K. Kodama, "Investigation on sensitized luminescence using evaporated films of 8-hydroxyquinolinato metal complexes", The Third International Symposium on Functional Dyes at UC Santa Cruz (1995).

Domestic conference

1. K. Fujii, H. Uekusa, J. Otani and M. Matsumura, "Structure determination of novel monoazo pigments from powder X-ray diffraction data", The 91st Annual Meeting of the Chemical Society of Japan, March (2011).

2. J. Otani, "DPP and quinacridone pigments, and latent pigment technology", Workshop on Hydrogen Bond: Its Functions, Electronic Structures and Applications, Yokohama, December (1998).

Patent applications related to colorants

1. T. Hisano and J. Otani, "5,6-Benzcoumarin compounds", Ueno Fine Chemicals

Industry, Co., Ltd., JP2008-081420 (2008).

2. T. Yamashita, T. Hisano, S. Mori and J. Otani, “2-Naphthol derivative and mono azo compound”, Ueno Fine Chemicals Industry, Co., Ltd. JP2008-013472 (2008).

3. T. Hisano and J. Otani, “Phthaloperinone compound”, Ueno Fine Chemicals Industry, Co., Ltd., JP2007-302782 (2007).

4. T. Hisano and J. Otani, “1,8-Dinitro-2-naphthol derivative and method for producing 1,8-diamino-2-naphtho derivative”, Ueno Fine Chemicals, Co., Ltd., JP2007-302603 (2007).

5. R. Ueno, J. Otani, T. Yamashita and T. Hisano, “Red ink composition for color filter”, Ueno Fine Chemicals Industry, Co., Ltd., WO2005/052074 (2005).

6. R. Ueno, J. Otani, T. Yamashita and T. Hisano, “Monoazo compound and method for producing same”, Ueno Fine Chemicals Industry, Co., Ltd., WO2004/108833 (2004).

7. J. Otani, H. Yamamoto, N. Dan, A. Iqbal and R. Moretti, “Electroluminescent device including diketopyrrolopyrroles”, Ciba Specialty Chemicals Holdings Inc., JP2006-319347 (2006).

8. K. Kunimoto, J. Otani, K. Kodama and H. Yamamoto, “Fluorescent maleimides and uses thereof”, Ciba Specialty Chemicals Holdings Inc., JP2003-509441 (2003).

9. J. Otani, H. Yamamoto, N. Dan, A. Iqbal and R. Moretti, “Electroluminescence element containing diketopyrrolopyrrole compound”, Ciba Specialty Chemicals Holdings Inc., JP2001-139940 (2001).

10. B. G. Devlin, J. Otani, K. Kunimoto, T. Deno, A. Iqbal and S. H. Eldin, “Process for the preparation of fluorescent compositions and their use”, Ciba Specialty Chemicals Holdings Inc. JP2001-511200 (2001).

11. B. G. Devlin, J. Otani, K. Kunimoto, A. Iqbal and S. H. Eldin, “Fluorescent host-guest system”, Ciba Specialty Chemicals Holdings Inc., JP2001-509832 (2001).

12. B. G. Devlin, J. Otani and K. Kunimoto, “Fluorescent chromophore, covalently linked to an organic support material”, Ciba Specialty Chemicals Holdings Inc.,

JP2001-509831 (2001).

13. J. Otani, M. Matsumura, K. Ikuta and T. Deno, “Organic electroluminescent element”, CIBA-GEIGY Japan Ltd., JP1994-045074 (1994).

Related research papers

1. J. Otani, “Diketopyrrolopyrrole pigments and quinacridone pigments: From the synthesis to current technology” (*a review paper in Japanese*), Nippon Gazo Gakkaishi, **37** (1998), pp.298-307.

2. I. Fujii, J. Otani, K. Kodama, H. Yamamoto and N. Hirayama, “Crystal structure of 2,5-bis-(3,5-dimethylbenzyl)-3,6-dinaphthalen-2-yl-2,5-dihydro-pyrrolo[3,4-c]pyrr ole-1,4-dione”, Analytical Sciences, **18** (2002), pp.221-222.

3. I. Fujii, J. Otani, K. Kodama, K. Kunimoto and N. Hirayama, “Crystal structure of 3,4-diphenyl-N-cyclohexylpyrrole-2,5-dione”, Analytical Sciences, **17** (2001), pp.1473-1474.

4. I. Fujii, J. Otani, K. Kodama, K. Kunimoto and N. Hirayama, “Crystal structure of 1,3,4-triphenyl-pyrrole-2,5-dione”, Analytical Sciences, **17** (2001), pp.1471-1472.

5. I. Fujii, J. Otani, K. Kodama, K. Kunimoto and N. Hirayama, “Crystal structure of 3,4-diphenyl-N-(2,6-bis(isopropyl)phenyl)pyrrole-2,5-dione”, Analytical Sciences, **17** (2001), pp.1249-1250.

6. I. Fujii, N. Hirayama, J. Otani and K. Kodama, “Crystal structure of tris(8-quinolinolato)aluminium (III)-ethyl acetate (1/0.5), Analytical Sciences, **12** (1996), pp 153-154.